Cosmic ray indirect detection

Valerio Vagelli
I.N.F.N. Perugia, Università degli Studi di Perugia
Corso di Fisica dei Raggi Cosmici A.A. 2016/2017

Cosmic Rays

Cosmic ray flux at Earth

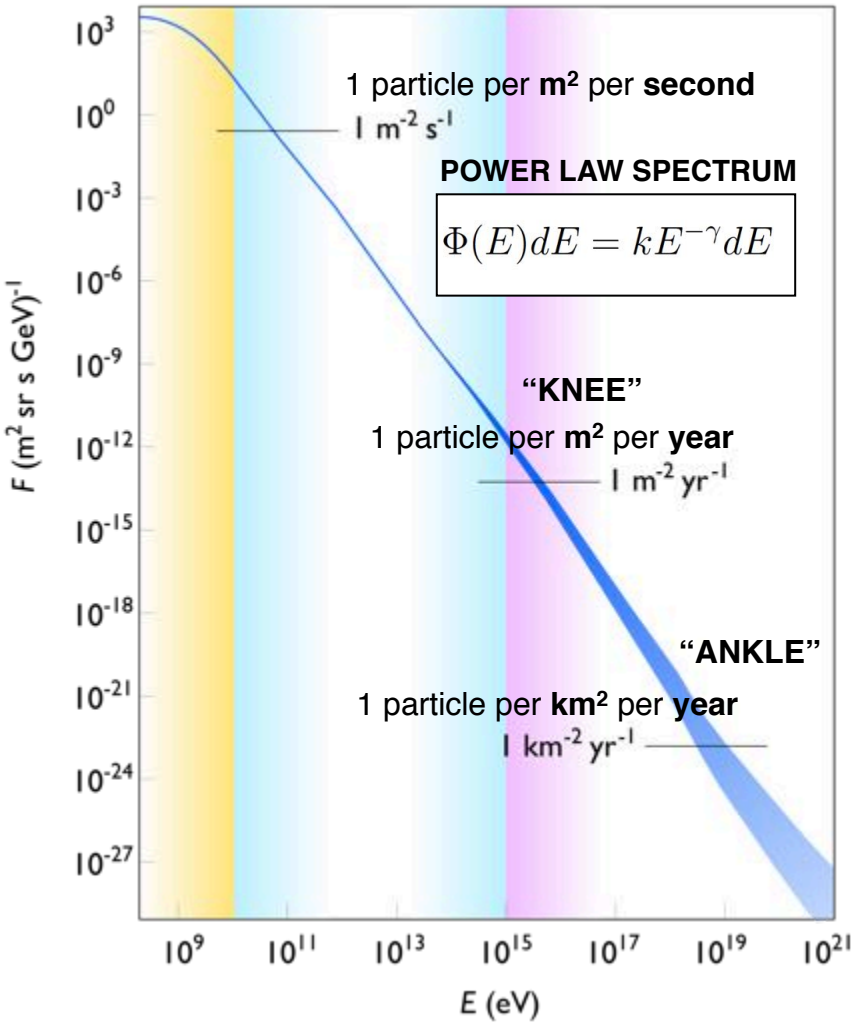

- Cosmic ray Flux: Intensity of CR in space per **unit of area, solid angle, time and energy**
- Energy range up to **10^{20} eV**
- Intensities spanning **30 orders of magnitude**
- Most of cosmic rays are **protons and nuclei**

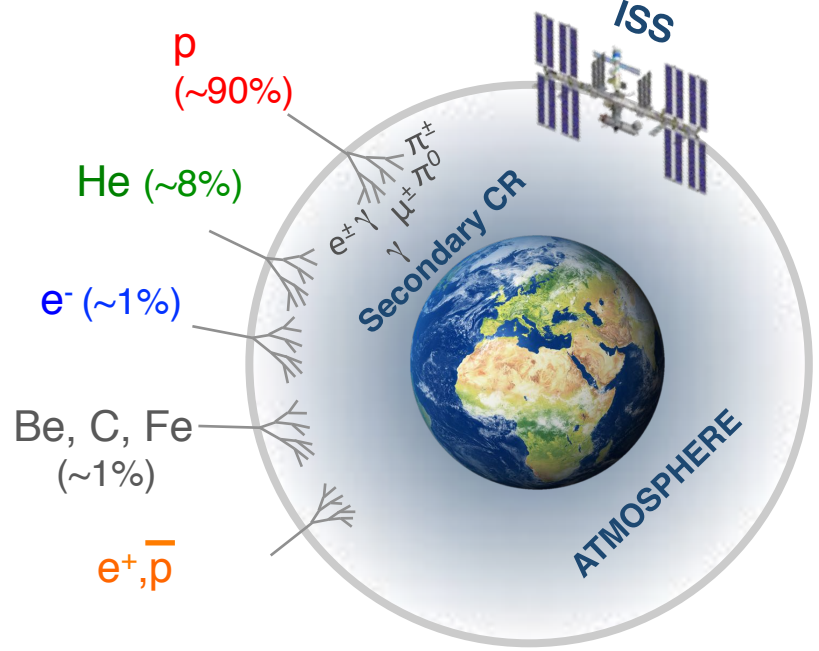

Cosmic Rays and Particle Physics

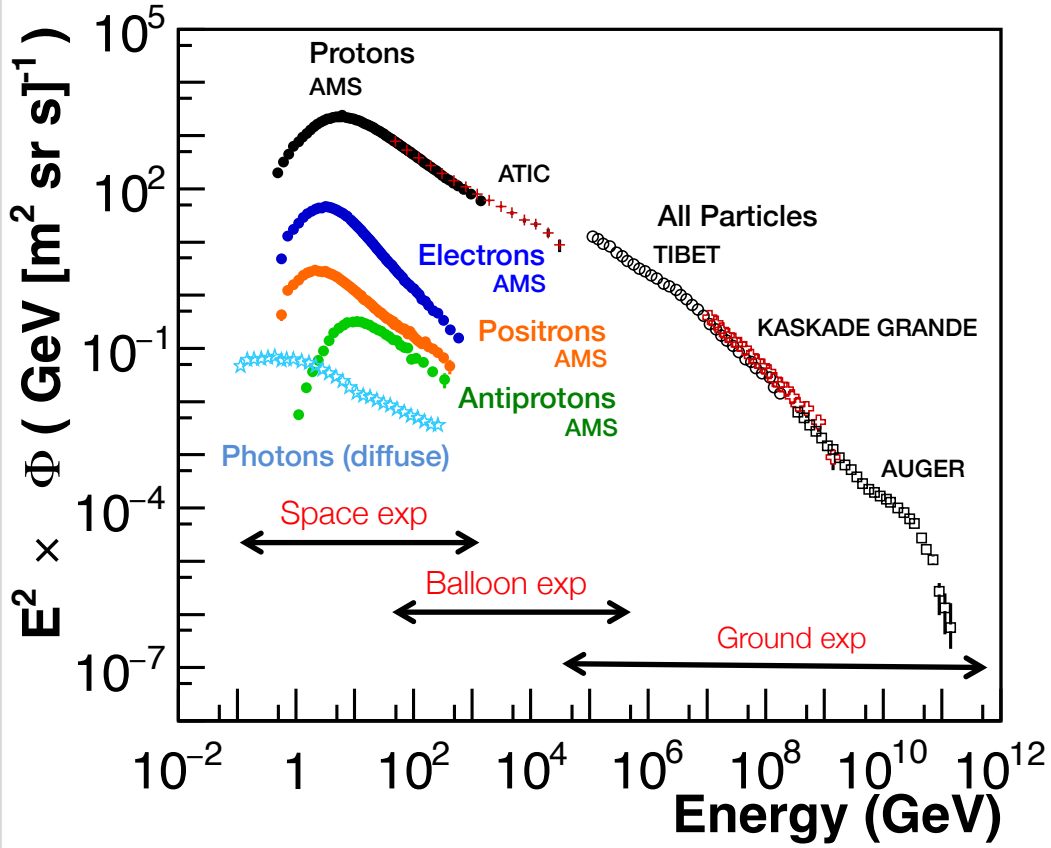

- Origin of very high energy CRs still not clear
- Many discussions about the origin of the “knee” and of the “ankle”
- Chemical composition above 1 TeV unknown
- Clear evidence of PeVatrons in the Universe

Cosmic Rays and Particle Physics

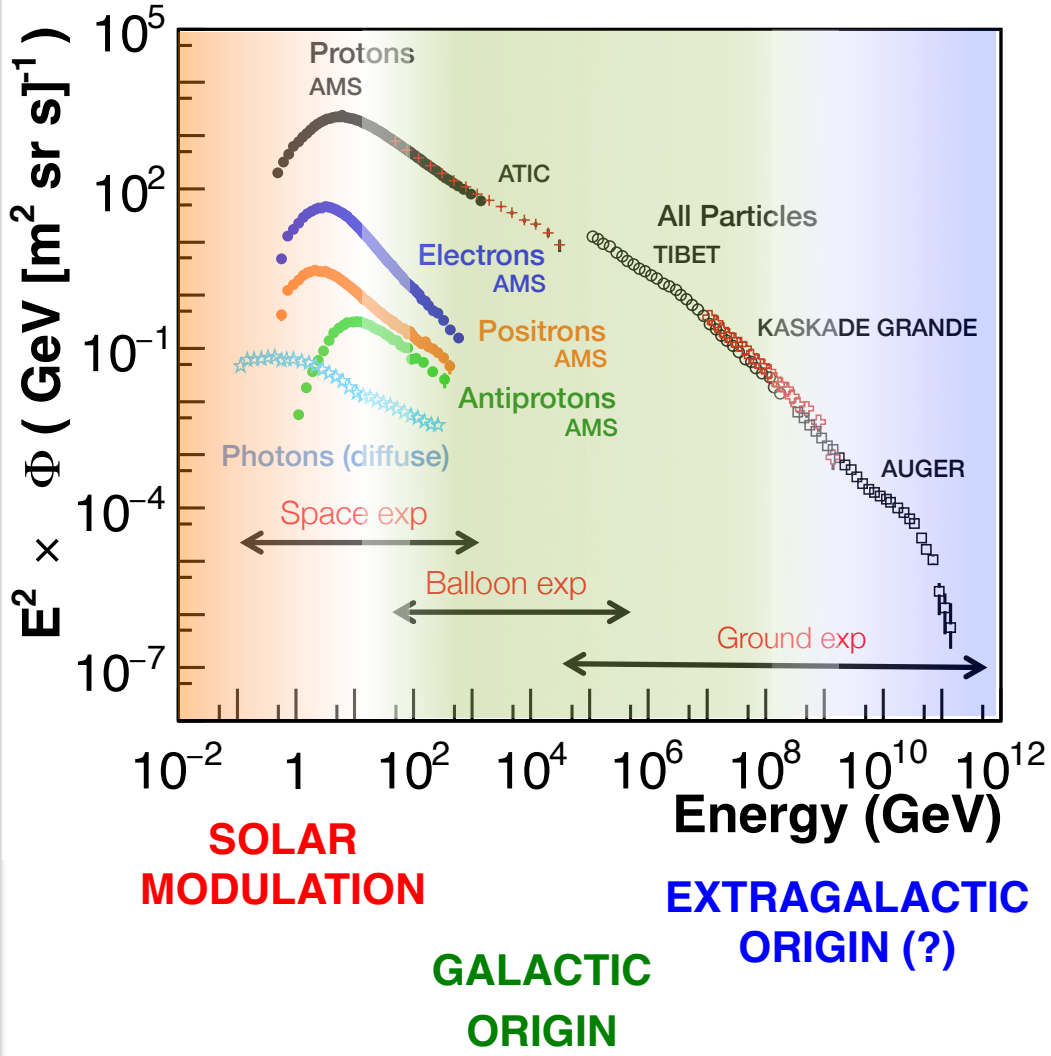

- Origin of very high energy CRs still not clear
- Many discussions about the origin of the “knee” and of the “ankle”
- Chemical composition above 1 TeV unknown
- Clear evidence of PeVatrons in the Universe

Ground based experiments

Charged CRs

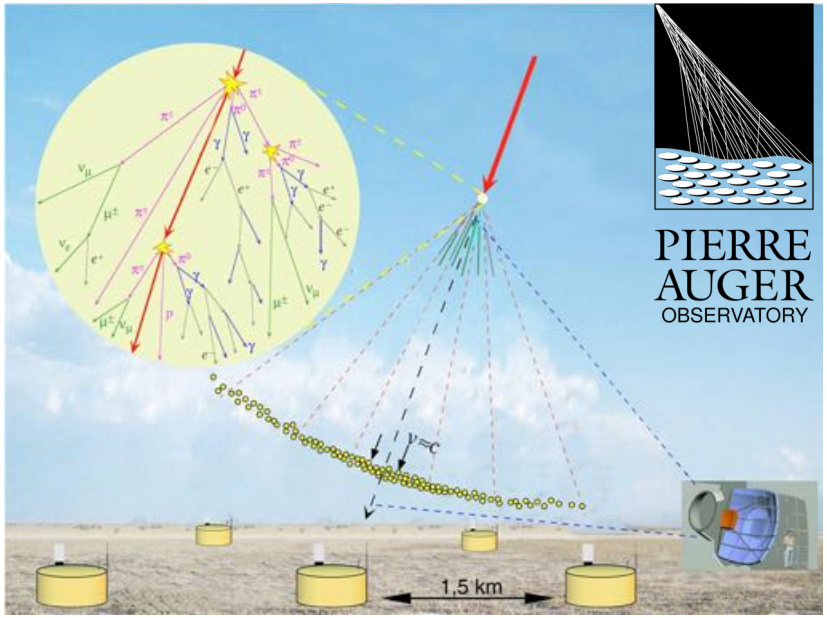

Gamma Rays

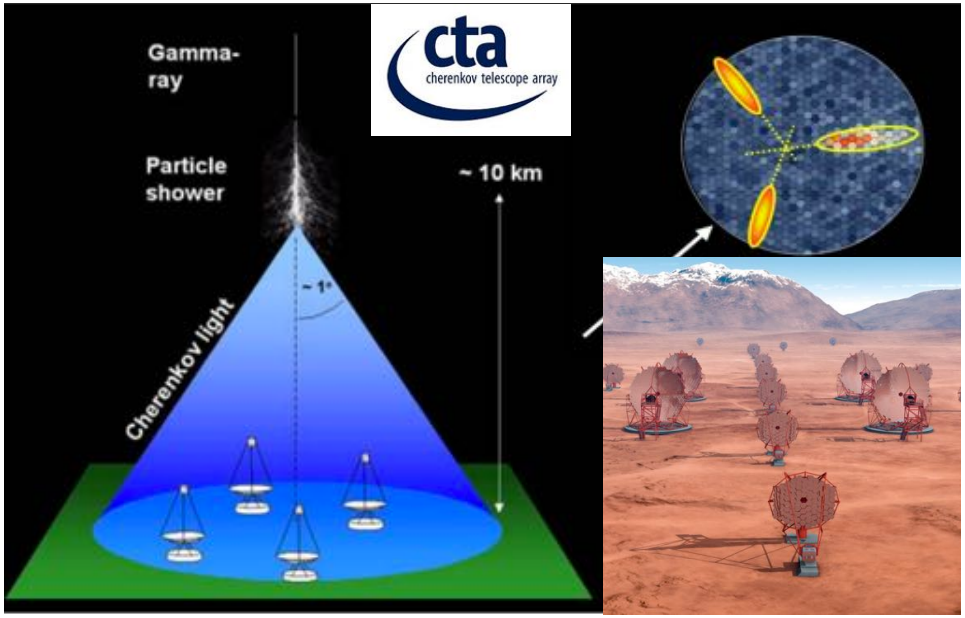

- √ Large collection areas → probe CR energies TeV –Eev ranges
- X Indirect measurements
  - Primary CR identified via the analysis of shower shapes and composition at ground (highly rely on MonteCarlo simulations)
  - Main systematics are the parametrization of X-sections at very high energies

The ultra-high-energy flux

Cosmic ray flux and energy scales

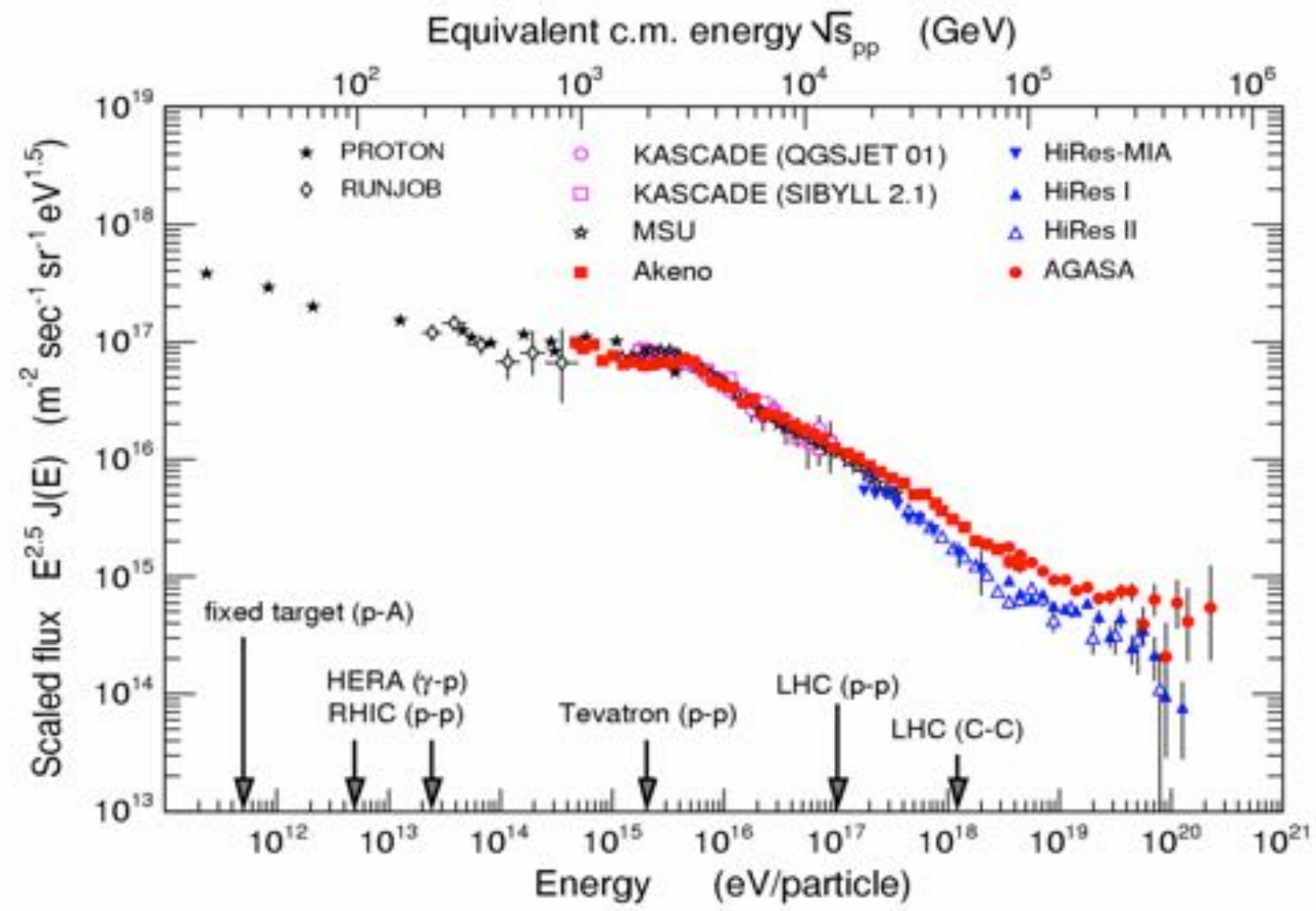

The indirect measurement principle

- When high energy cosmic rays enter the atmosphere, they initiate **particle showers**. Secondary particles may reach the ground and be detected by ground experiments. The **atmosphere** is used as a huge calorimeter.

- High energy CR fluxes are faint, so we need **large (up to O(1000) km^2) collection areas** to maximize the statistics. Luckily, showers may extend over more than 100m^2.

- The primary particle properties is inferred from the properties of the shower sampled at ground. Indirect measurements are characterized by uncertainties with are typically one order of magnitude worse than direct detection experiments.

The indirect measurement principle

The Pierre Auger Observatory in Umbria

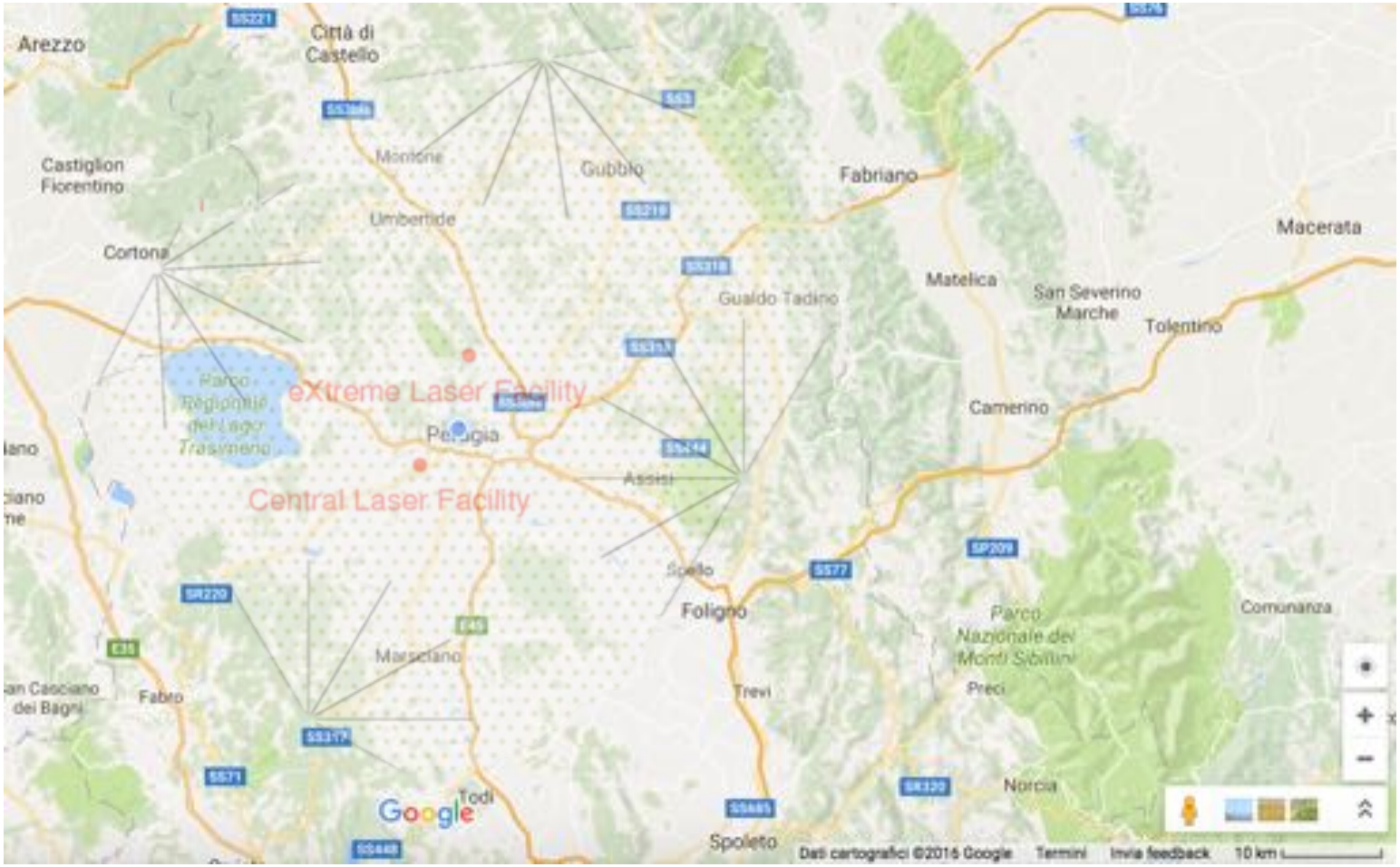

Particle showers

- Electromagnetic shower development are defined by the interactions in matter of high energy photons and electrons

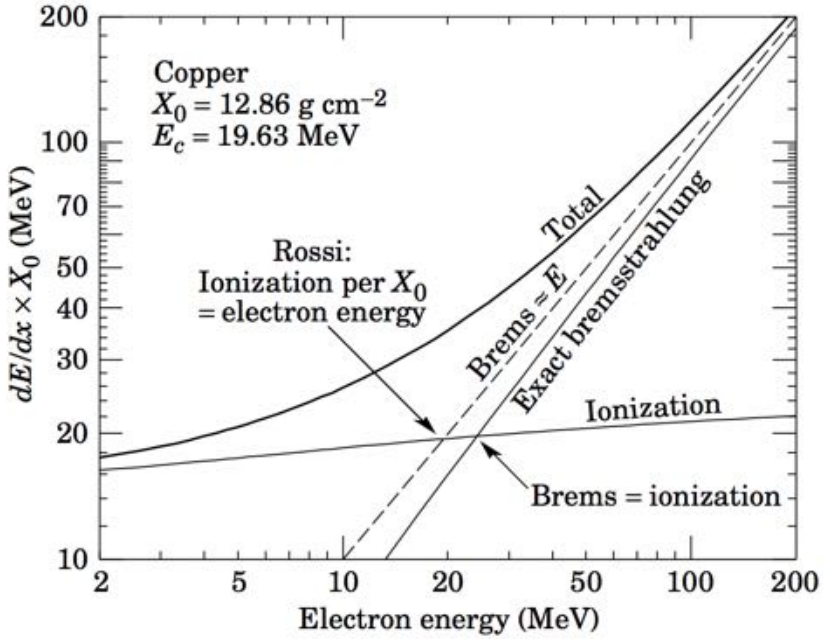

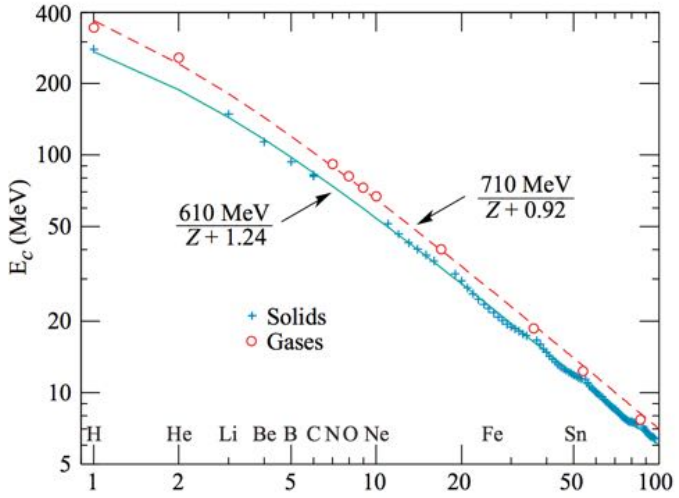

Material		X_0 (g cm^{-2})	λ_I (g cm^{-2})	E_c (MeV)
Active detectors	NaI	9.5	151	12.5
	BGO	8.0	157	7
Passive absorbers	Fe	13.8	132	28
	Pb	6.4	194	9.5
	U	6.0	199	9
Air [STP]	Mixture	36.7	90	86

Critical energy for electrons in air ~ 100 MeV (for muons $Ec(\mu) = (m_\mu/m_e)^2\, Ec(e)$)
Interaction length for electrons in air ~ 30 g/cm^2
Above critical energy, electrons loose energy via Bremstrahlung. Below, they ionize.

Particle showers

- Electromagnetic shower development are defined by the interactions in matter of high energy photons and electrons

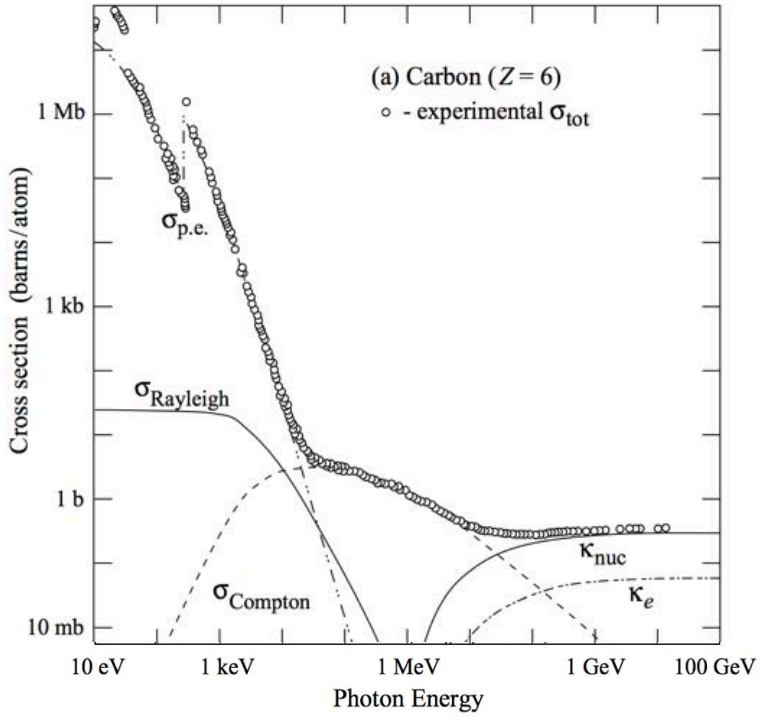

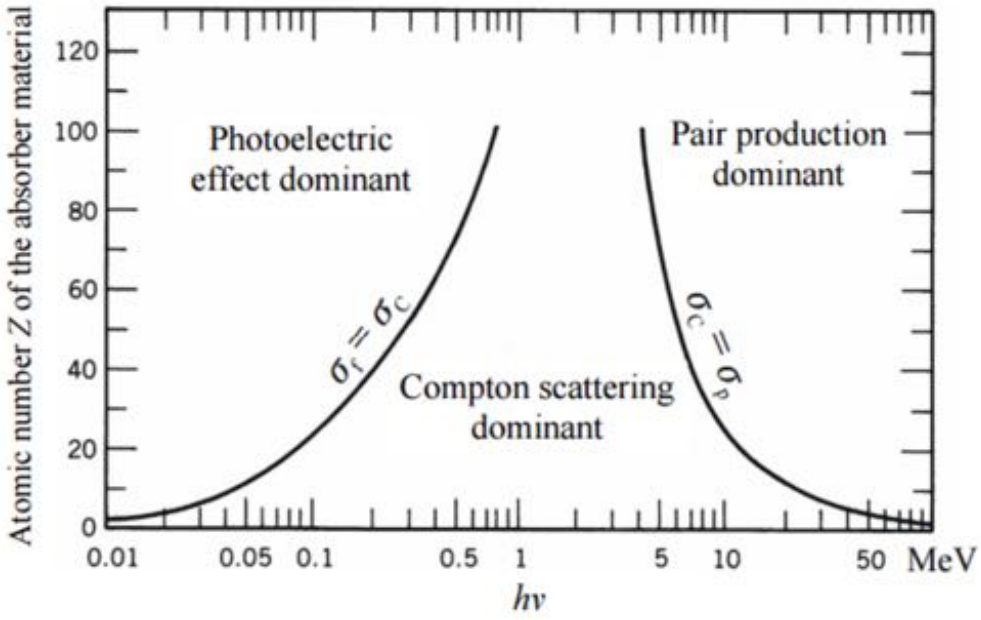

X0 (p.p) = 9/7 X0 (Bremms)
Above critical energy, photons convert in e+e- with a typical length of X0 (p.p.)
I(x) = I(0) exp(-X/X0)

Particle showers

- The Heitler model can be used to understand the basic properties of electromagnetic showers

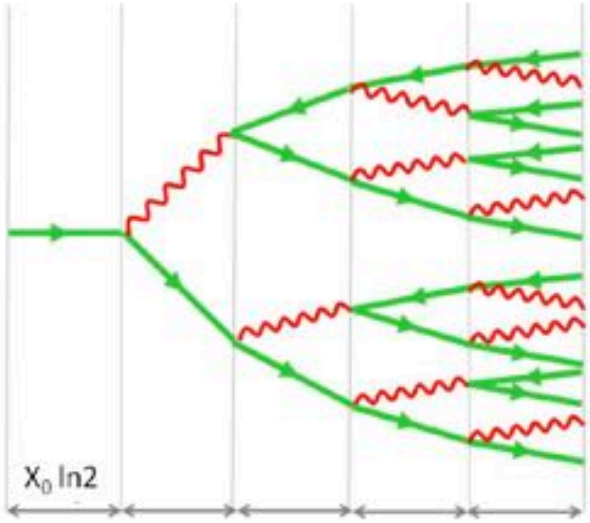

d=	1	2	3	4	5
N=	2	4	8	16	32
E=	1/2	1/4	1/8	1/16	1/32

The electron losses half of his energy when : $R = X_0 \ln(2)$

Define the scale variables: $t = z/X_0 \quad y = E_0/E_c$

Total number of produced electrons after z = n R : $N(z) = 2^n$

Mean energy for each particle : $E(z) = E_0/2^n$

Particle creation in shower stops when E < Ec : $n_c = \frac{1}{\ln 2} \ln\left(\frac{E_0}{E_c}\right)$

Maximum depth : $z_{max} = X_0 \ln\left(\frac{E_0}{E_c}\right)$

Numer of particle at zmax : $N_{max} = E_0/E_c$

Fig. 4.2. Toy model evolution of an electromagnetic cascade. At each step of the cascade the number of particles is multiplied by two, through either pair creation or single photon bremsstrahlung. Backward arrows indicate a positron positron, as in Feynman diagrams. The evolution stops when individual particle energies fall below the critical energy E_c. The number N of particles at each step d and the average particle energy E in the Heitler's model are also indicated. Adapted from [4ww01]

Particle showers

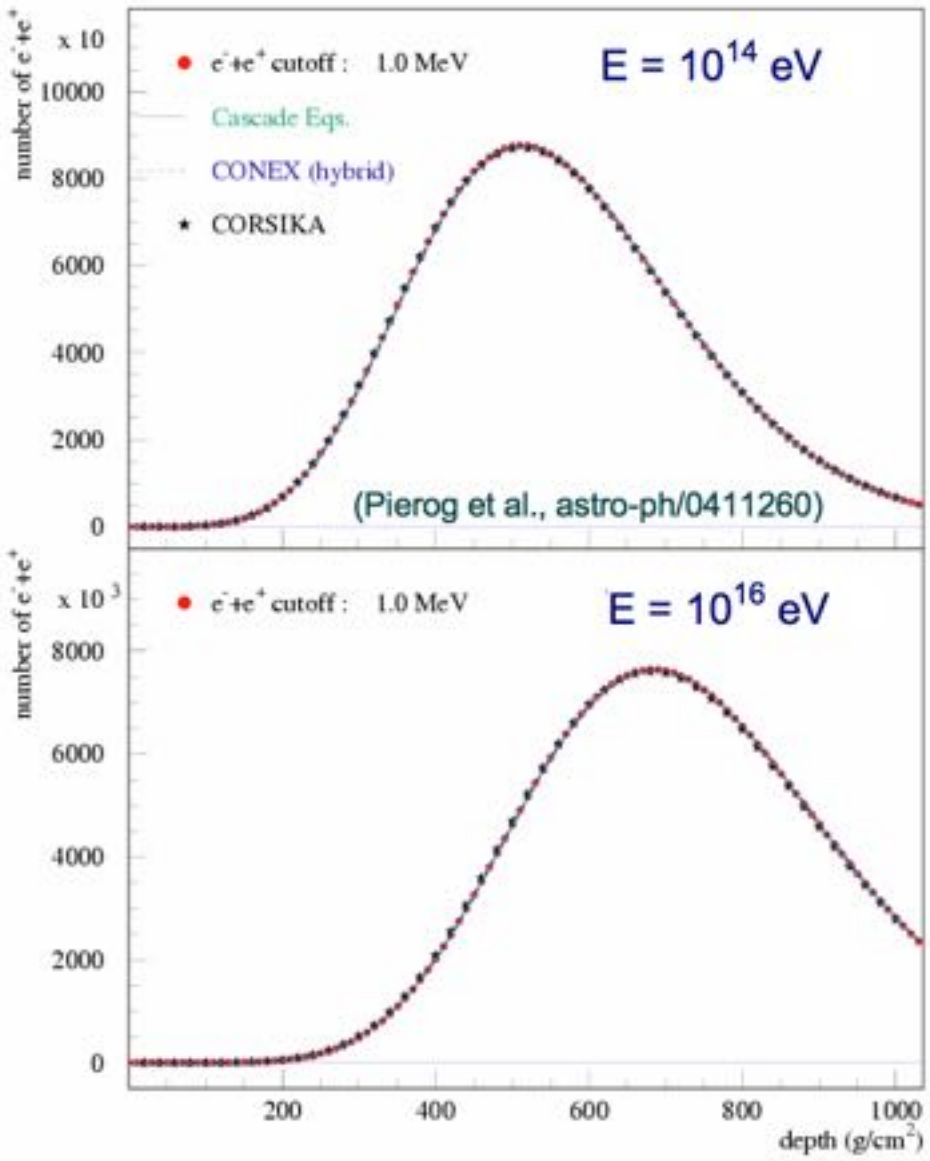

Electromagnetic shower can be well modelled using semi-analitical parametrizations or MonteCarlo simulations

Atmosphere

Altitude (km)	Vertical depth (g/cm^2)	Local density (10^{-3} g/cm^3)	Molière unit (m)	Electron Cherenkov threshold (MeV)	Cherenkov angle (°)
40	3	3.8×10^{-3}	2.4×10^{4}	386	0.076
30	11.8	1.8×10^{-2}	5.1×10^{3}	176	0.17
20	55.8	8.8×10^{-2}	1.0×10^{3}	80	0.36
15	123	0.19	478	54	0.54
10	269	0.42	223	37	0.79
5	550	0.74	126	28	1.05
3	715	0.91	102	25	1.17
1.5	862	1.06	88	23	1.26
0.5	974	1.17	79	22	1.33
0	1,032	1.23	76	21	1.36

Energy loss of electron: $$\frac{\mathrm{d}E}{\mathrm{d}X} = -\alpha - \frac{E}{X_0}$$

Critical energy: $E_c = \alpha X_0 \sim 85\,\mathrm{MeV}$

Radiation length: $X_0 \sim 36\,\mathrm{g/cm^2}$

Particle showers

- Showers initiated by hadronic interactions are more complicated

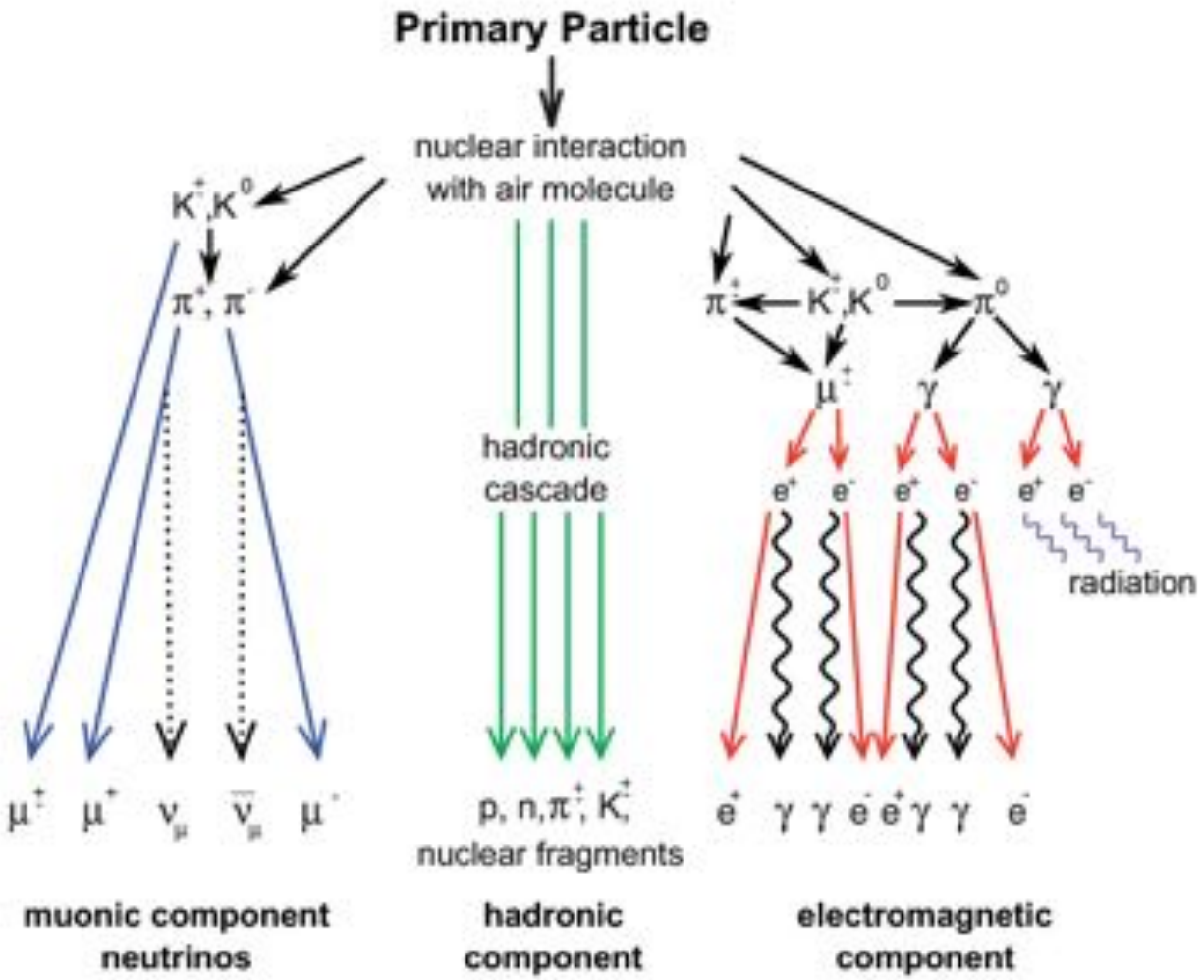

Particle showers

$$p + N \longrightarrow \pi^{\pm}, \pi^{0}, K^{\pm}, K, p, n, +....(exotic)$$

$$\pi^{0} \longrightarrow \gamma\gamma \qquad \tau_{\pi} = 1.8 \cdot 10^{-16} s$$

$$\pi^{\pm} \longrightarrow \mu^{\pm}\nu_{\mu} \qquad \tau_{\pi} = 2.5 \cdot 10^{-8} s$$

$$\mu^{\pm} \longrightarrow e^{\pm}\nu_{e}\nu_{\mu} \qquad \tau_{\pi} = 2.2 \cdot 10^{-6} s$$

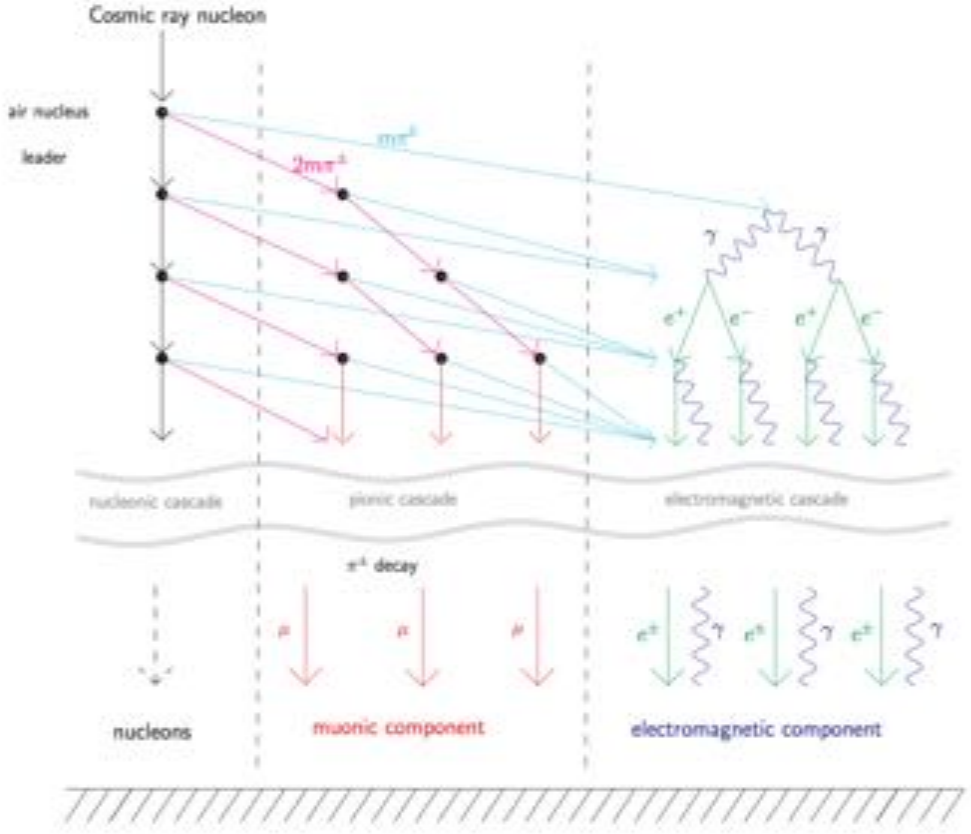

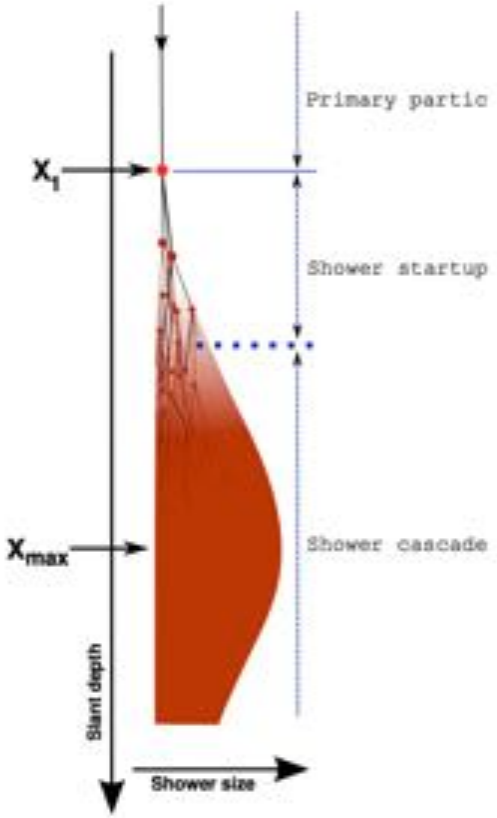

Particle showers

$$p + N \longrightarrow \pi^{\pm}, \pi^{0}, K^{\pm}, K, p, n, +....(exotic)$$

$$\pi^{0} \longrightarrow \gamma\gamma \qquad \tau_{\pi} = 1.8 \cdot 10^{-16} s$$

$$\pi^{\pm} \longrightarrow \mu^{\pm}\nu_{\mu} \qquad \tau_{\pi} = 2.5 \cdot 10^{-8} s$$

$$\mu^{\pm} \longrightarrow e^{\pm}\nu_{e}\nu_{\mu} \qquad \tau_{\pi} = 2.2 \cdot 10^{-6} s$$

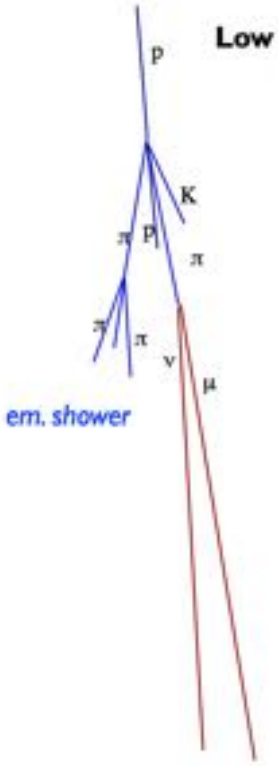

Typical energies above which particles interact

$$E_{\pi^{\pm}} \sim 30\,\mathrm{GeV}$$

$$E_{K} \sim 200\,\mathrm{GeV}$$

$$E_{\pi^{0}} \sim 10^{19}\,\mathrm{eV}$$

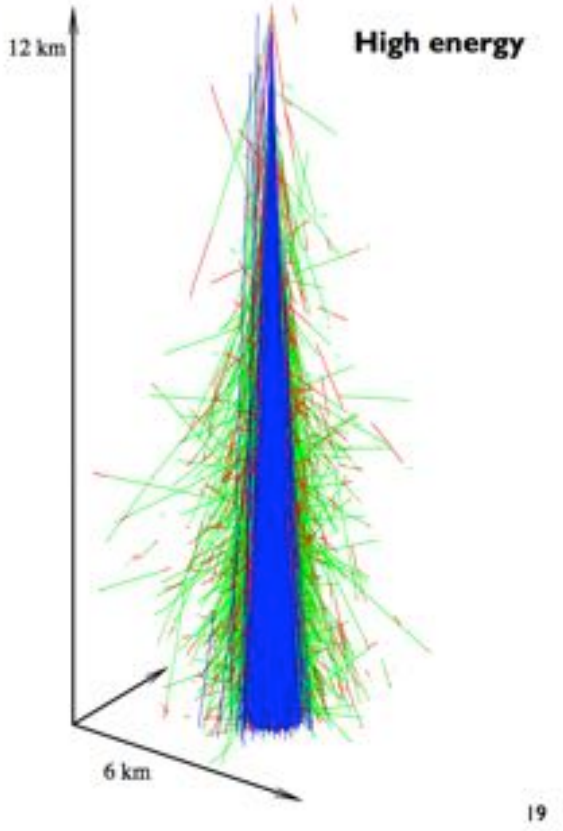

Particle showers

$$p + N \longrightarrow \pi^{\pm}, \pi^{0}, K^{\pm}, K, p, n, +....(exotic)$$
$$\pi^{0} \longrightarrow \gamma\gamma \qquad \tau_{\pi} = 1.8 \cdot 10^{-16} s$$
$$\pi^{\pm} \longrightarrow \mu^{\pm}\nu_{\mu} \qquad \tau_{\pi} = 2.5 \cdot 10^{-8} s$$
$$\mu^{\pm} \longrightarrow e^{\pm}\nu_{e}\nu_{\mu} \qquad \tau_{\pi} = 2.2 \cdot 10^{-6} s$$

Hadronic shower dynamics can be understood using a very semplicistic model.

- After each interaction, the primary nucleon carries a fraction 1-f (inelasticity) of its initial energy E_0, and the rest f is distributed to the N_π pions.
- The multiplicity N_π is a function of sqrt(s), and $N_{\pi+/-} \sim E^{0.2}$ (from lab mesurements, $N_{\pi+/-}=10$ for $E_0=100$GeV)
- After k interactions, the primary carries $(1-f)^k E_0$ energy. The rest is spread among N_π pions, each having around $E_0/(N_\pi)^k$
- π_0 decay istantly, transferring their energy to the electromagnetic component of the shower
- $\pi^{+/-}$ decay slower, and the decay probability concurs with the interaction probability. If $E_\pi > E_\pi^{crit} \sim 20$ GeV, pions continue to interact. Otherwise, they decay transferring their energy to the muonic and invisible component of the shower

Particle showers

$$p + N \longrightarrow \pi^{\pm}, \pi^{0}, K^{\pm}, K, p, n, +....(exotic)$$

$$\pi^{0} \longrightarrow \gamma\gamma \qquad \tau_{\pi} = 1.8 \cdot 10^{-16} s$$

$$\pi^{\pm} \longrightarrow \mu^{\pm}\nu_{\mu} \qquad \tau_{\pi} = 2.5 \cdot 10^{-8} s$$

$$\mu^{\pm} \longrightarrow e^{\pm}\nu_{e}\nu_{\mu} \qquad \tau_{\pi} = 2.2 \cdot 10^{-6} s$$

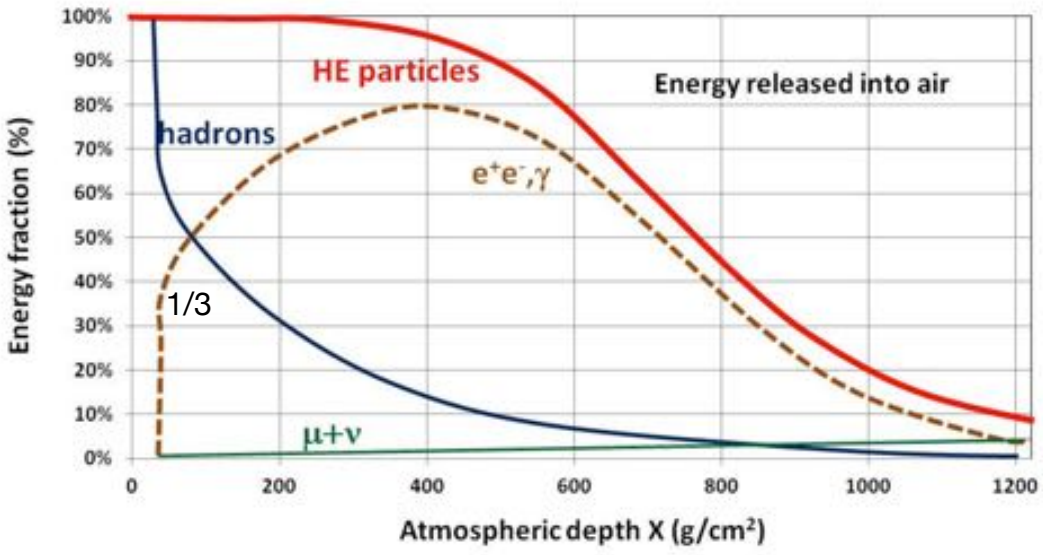

Fig. 4.5. Fraction of energy transferred to the different components of the cascade induced by a primary proton of 10^{19} eV. Part of the energy is released into air by excitation/ionization processes. The top graph uses a linear scale for the energy fraction; the bottom uses a log scale for a better visualization of the "older" part of the shower

Particle showers

- Muons are produced by decaying low energy pions.
  $N\mu = (E_0/E_\pi^{crit})^\beta$, $\beta \sim 0.9$
- Electrons are produced by the decay of π_0. The electromagnetic energy fraction amounts to $f_{em}=1 - (E_0/E_\pi^{crit})^{1-\beta}$. f_{em} amounts to ~70% at 10^{15} eV and 95% at 10^{20}eV
- The hadronic shower is a superimposition oh em and hadronic sub-showers.
  The shower maximum X_{max} occurs typically higher in the atmosphere than that initiated by a photon with the same energy E_0, by at least 1.5~2 X_0 (energy dependent)

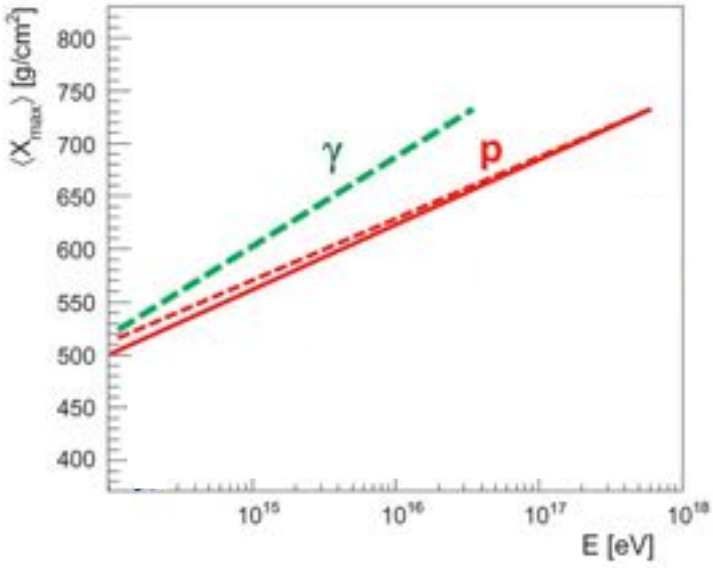

Particle showers

- The number of electrons at the shower maximum is a function of the primary energy $N_e = 6x10^5(E_0/PeV)$.
- At ground, we tipically measure $e^{+/-}$ below E_c (with O(10) MeV energy), muons with energies 3-4 GeV, and a small fraction of pions, neutrinos.

- The shower dynamics is clearly very complex. However, it has been proved that: the energy of the primary (E_0) can be estimated by measuring the number of electrons (N_e) and muons (N_μ) and it is proportional to a simple function of N_e and N_μ

Nuclei-induced showers

- Superimposition model: the shower induced by a nucleon with mass number A and energy E_0 is equivalent to the superimposition of A showers initiated be A=1 (proton) primaries with energy E_0/A.

- The e.m. content of proton-shower or nuclei-shower is the same. Cannot be used to distinguish them
- The muon content increases slowly as function of A. $N_\mu^{(A)} \sim A^{(1-\beta)} N_\mu^{(p)}$, $(1-\beta) \sim 0.1$

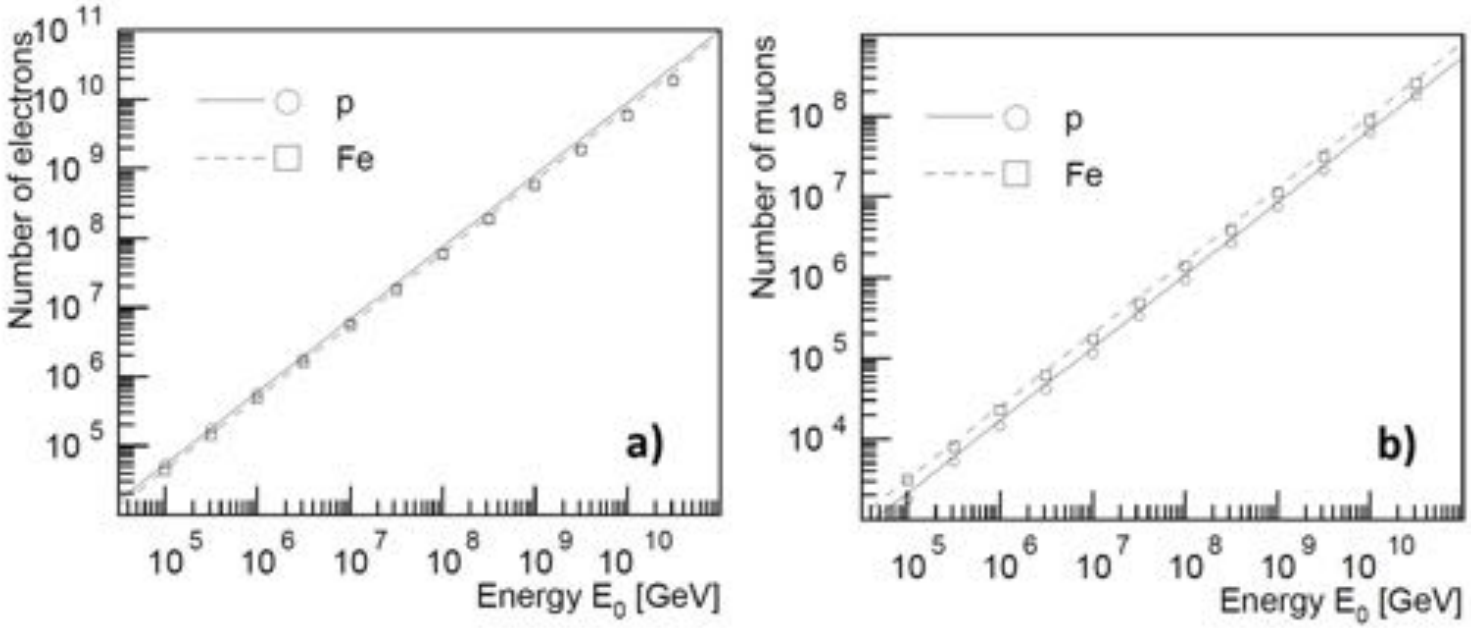

Nuclei-induced showers

- Superimposition model: the shower induced by a nucleon with mass number A and energy E_0 is equivalent to the superimposition of A showers initiated be A=1 (proton) primaries with energy E_0/A.

- The e.m. content of proton-shower or nuclei-shower is the same. Cannot be used to distinguish them
- The muon content increases slowly as function of A. $N_\mu^{(A)} \sim A^{(1-\beta)}\ N_\mu^{(p)}$, $(1-\beta)\sim 0.1$

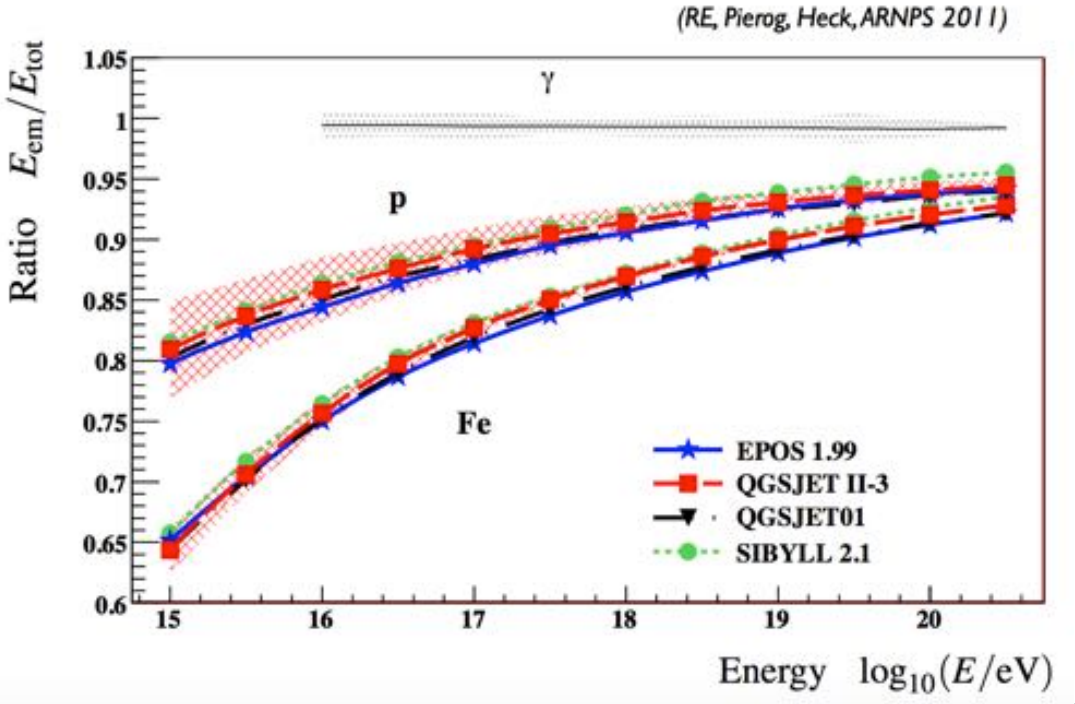

Ratio of e.m. energy content wrt total shower energy

Nuclei-induced showers

- Superimposition model: the shower induced by a nucleon with mass number A and energy E_0 is equivalent to the superimposition of A showers initiated be A=1 (proton) primaries with energy E_0/A.

- Nuclei have higher cross-sections, $\sigma \sim A^{2/3}$, so $\lambda^{(A)} \sim A^{-2/3}\lambda^{(p)}$. Nuclei-induced showers initiate earlier in the atmosphere, with $X_{max}^{(A)} \sim X_{max}^{(p)} - X_0 \ln A$

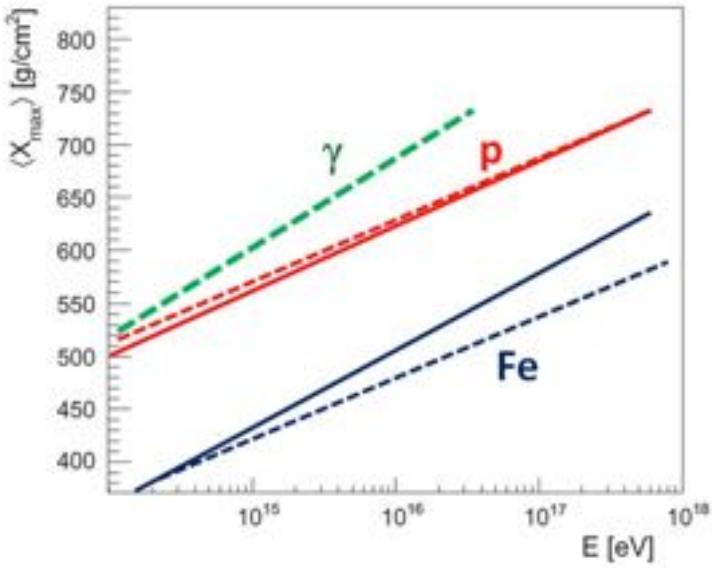

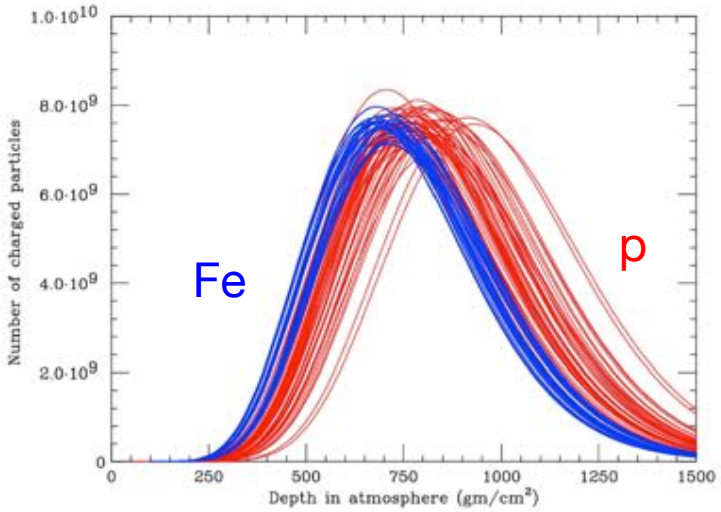

Fig. 4.9. Simulation of the longitudinal profile produced with the CORSIKA code for 50 proton-induced (red) and 50 iron-induced (blue) showers. The same total energy of 10^{19} eV is assumed. Shower-to-shower fluctuations on $N_{e_{max}}$ and X_{max} are evident. From [4De08]

Shower numerical simulations

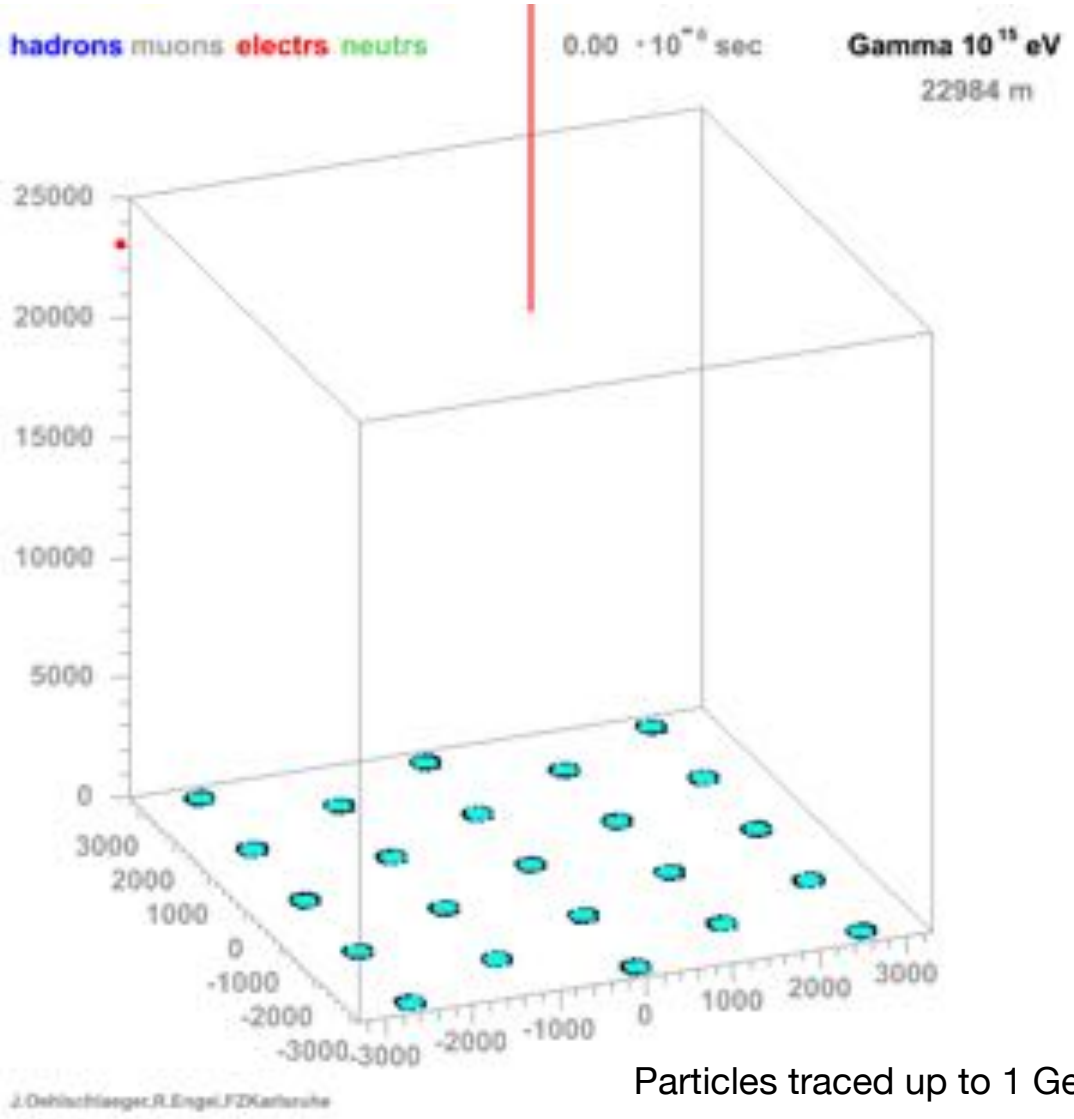

Particles traced up to 1 GeV

Shower numerical simulations

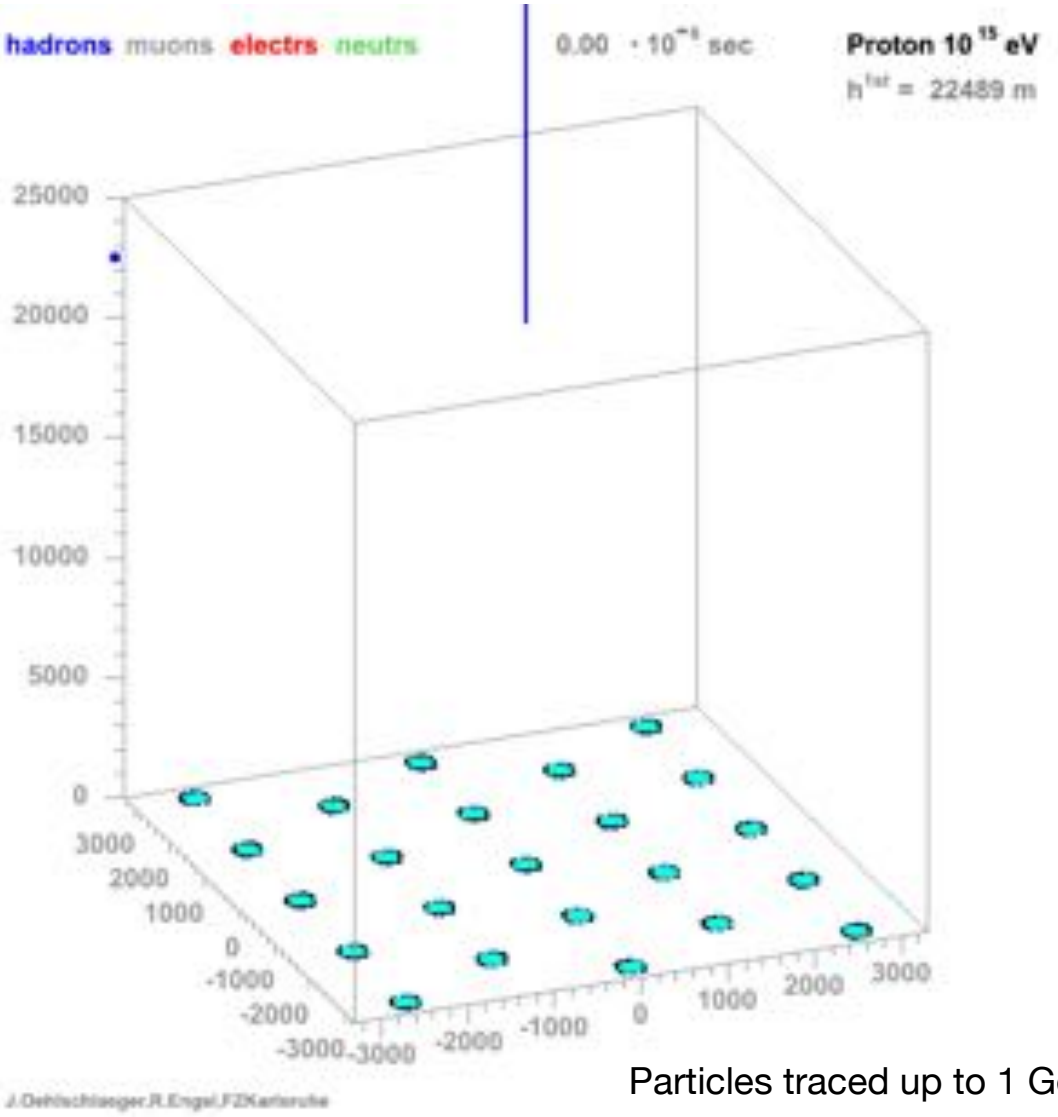

Particles traced up to 1 GeV

Shower numerical simulations

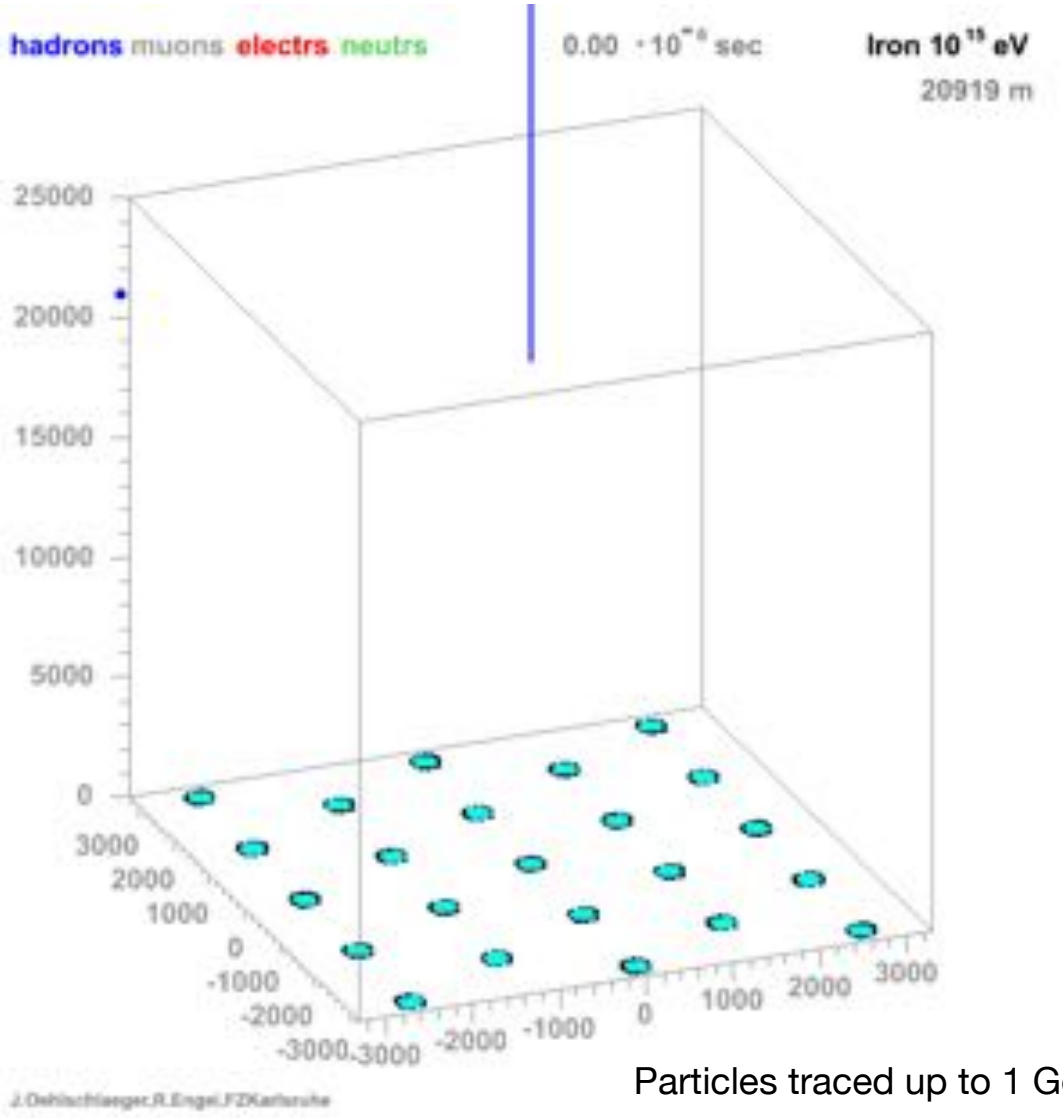

Particles traced up to 1 GeV

Shower numerical simulations

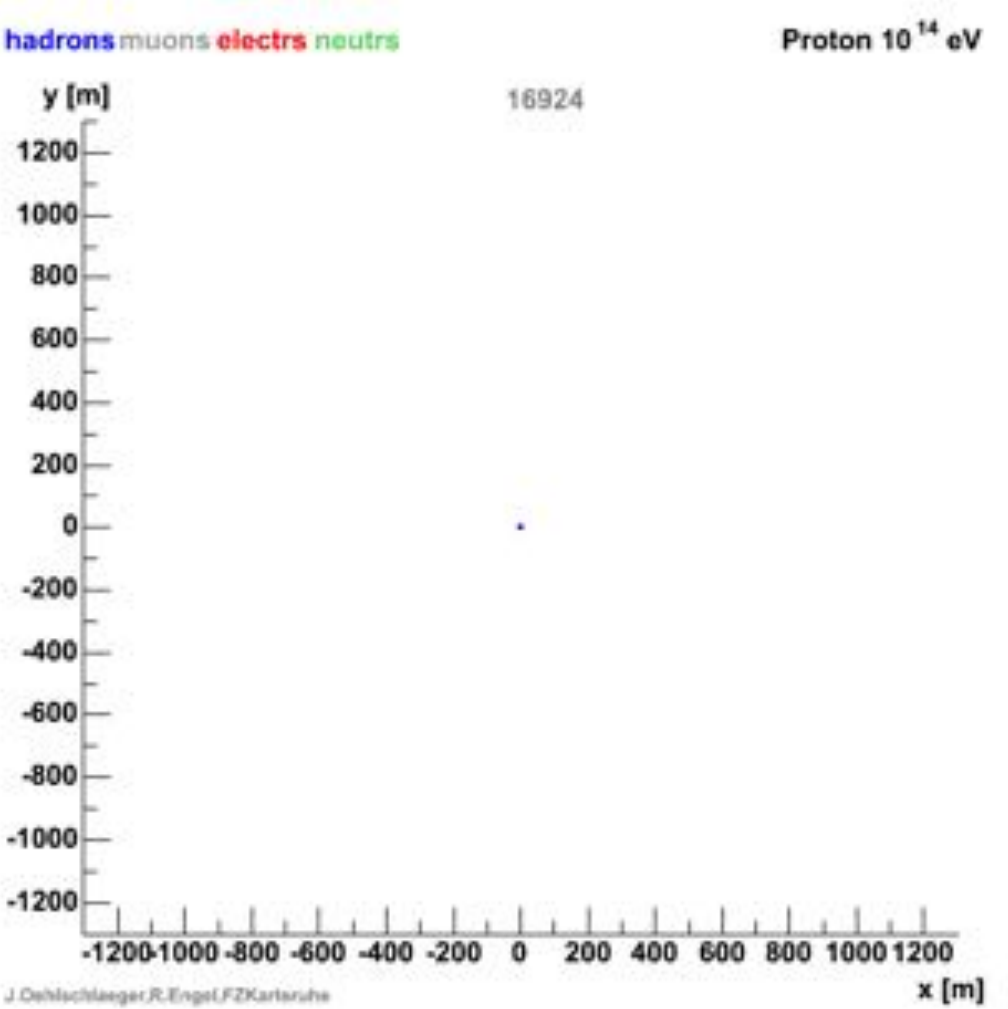

Particles traced up to 0.1 GeV

Shower numerical simulations

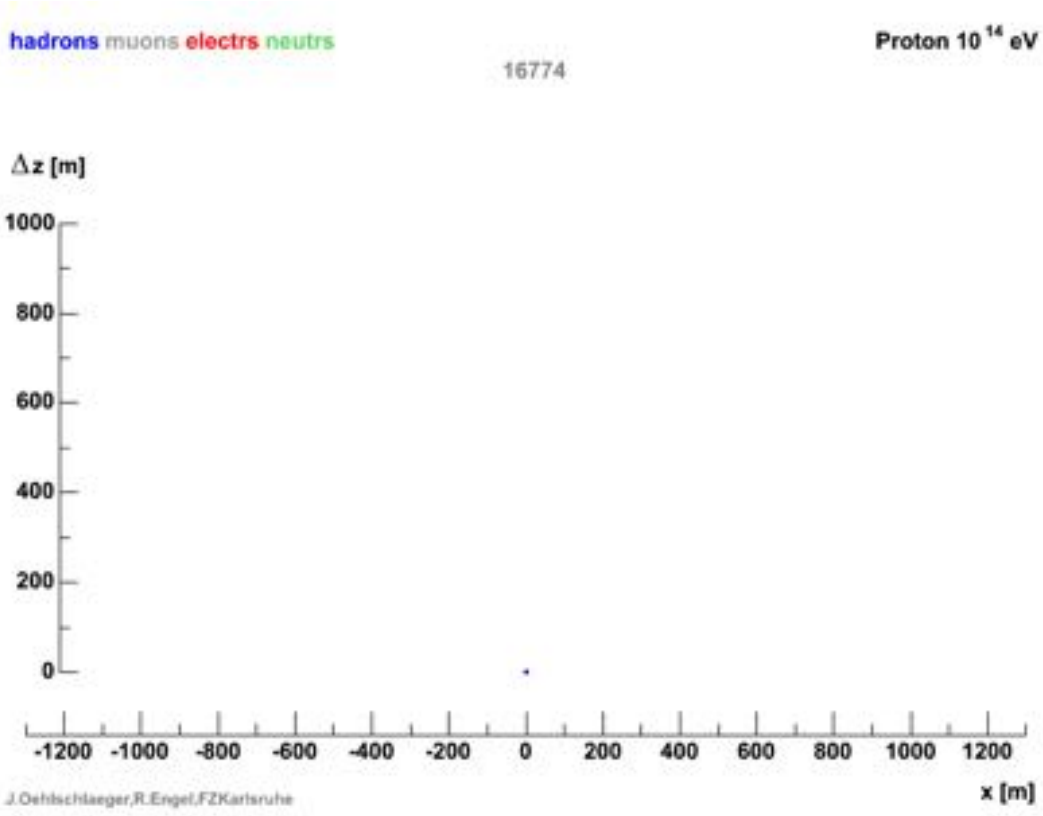

Particles traced up to 0.1 GeV

Shower numerical simulations

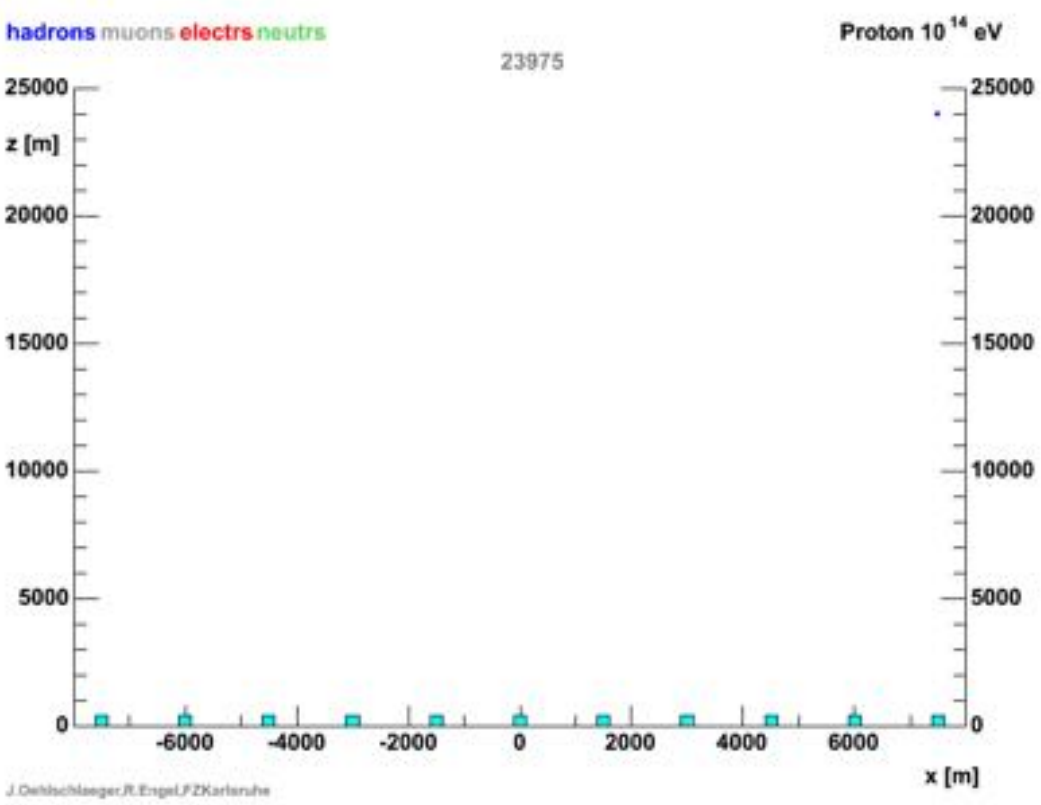

Particles traced up to 0.1 GeV

Particle showers

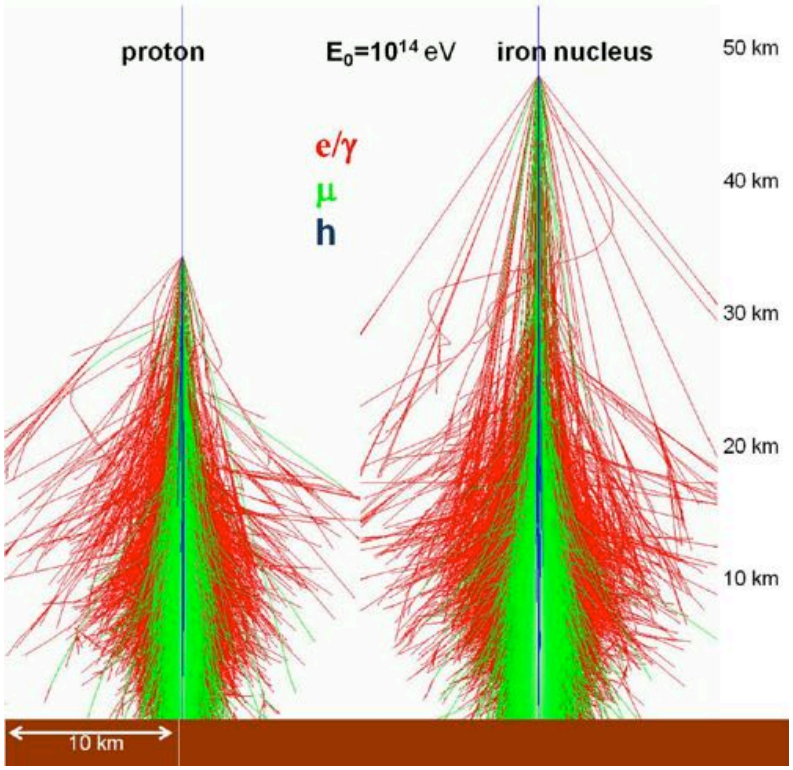

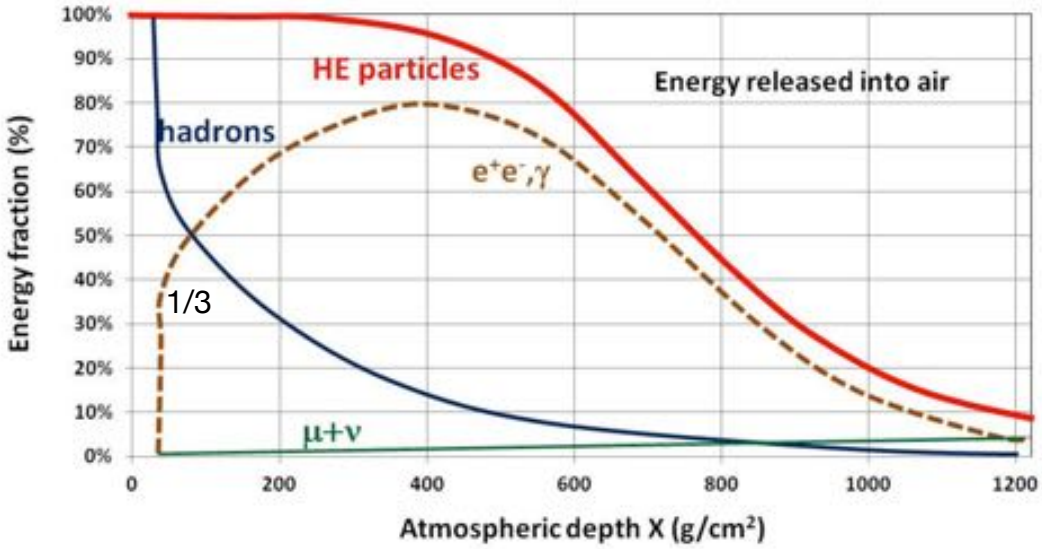

Fig. 4.5. Fraction of energy transferred to the different components of the cascade induced by a primary proton of 10^{19} eV. Part of the energy is released into air by excitation/ionization processes. The top graph uses a linear scale for the energy fraction; the bottom uses a log scale for a better visualization of the "older" part of the shower

Particle showers

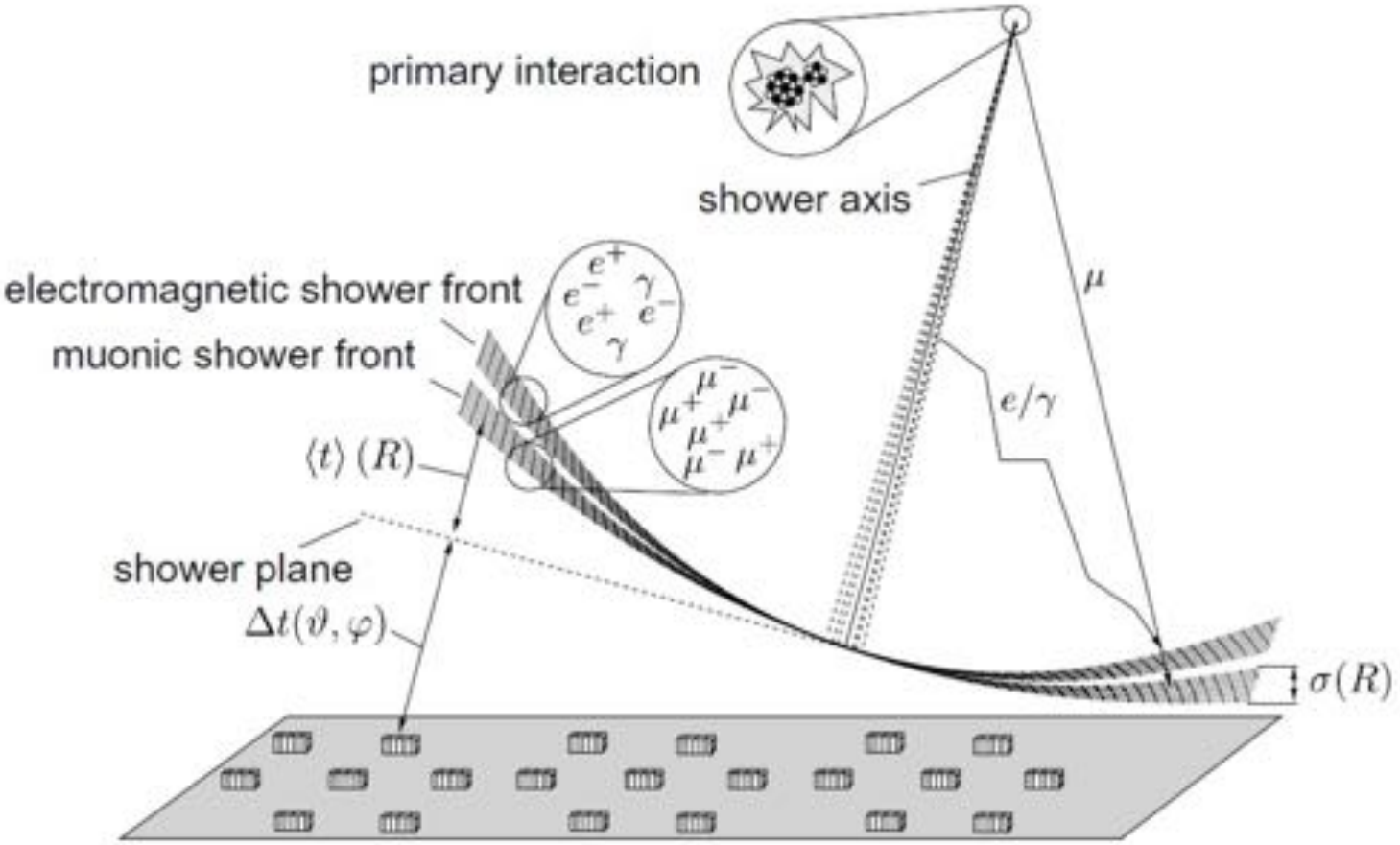

Muons are produced higher in the atmosphere, are more energetic and suffer less multiple scattering than electrons. Two different shower fronts build up. This effect can be used to separate the electronic and muonic content of the shower. Typical time delays in the shower core is ~5ns.

Particle showers

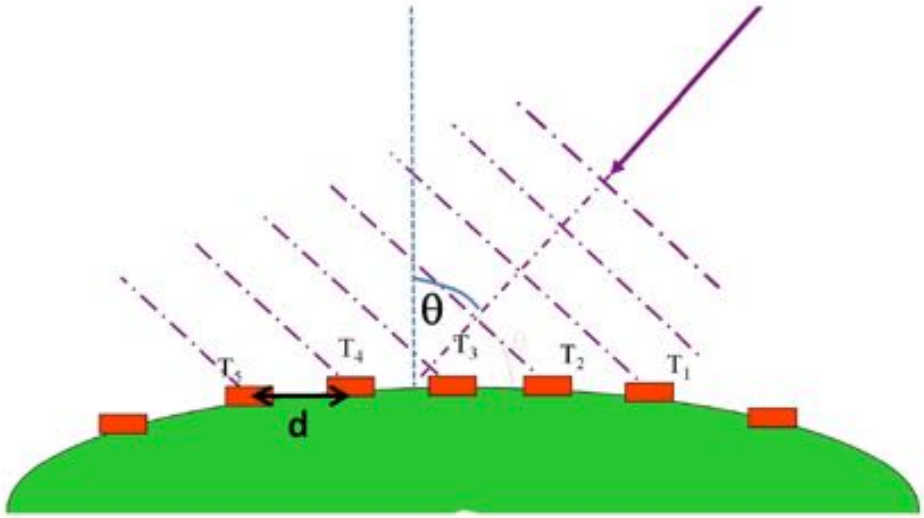

The reconstruction of the shower incoming direction is based on the different measurement times on several counters. Due to statistical fluctuations, many counters are used and the direction is estimated using best-fit techniques.

Detector Arrays

- Extensive showers are detected combining the measurements of several detector **units** spread over a **wide area** (array)
- Different detectors are used depending on the observable to be measured
- If possible, the measurement of more than one observable provides an improvement in the primary particle property accuracy
- Typical detectors used:
  - Cherenkov tanks
  - Cherenkov telescope
  - Fluorescence telescope
  - Muon detectors

Detector Arrays

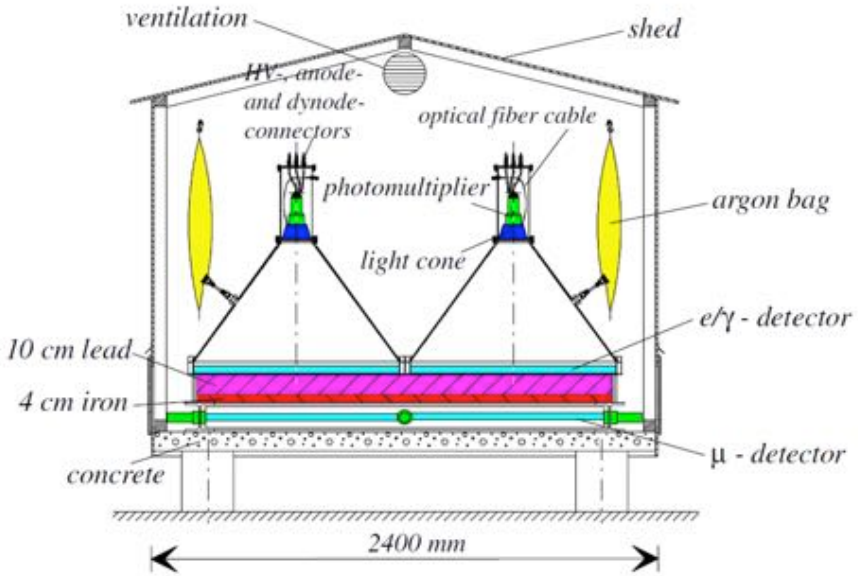

Cherenkov radiation

- In addition to the direct detection of the shower components, it is interesting to measure indirectly to amount of particles in the shower.
- Cherenkov radiation
  - Particle travelling faster than the speed of light yield a cone of Cherenkov radiation, with a typical angular aperture of O(1)°
  - The light yield is emitted in a directional cone, with a yield of O(10) photon/m for each shower particle above threshold. The number of emitted photon is proportional to the number of particles in the shower, therefore to the primary particle energy

Imaging Cherenkov telescope

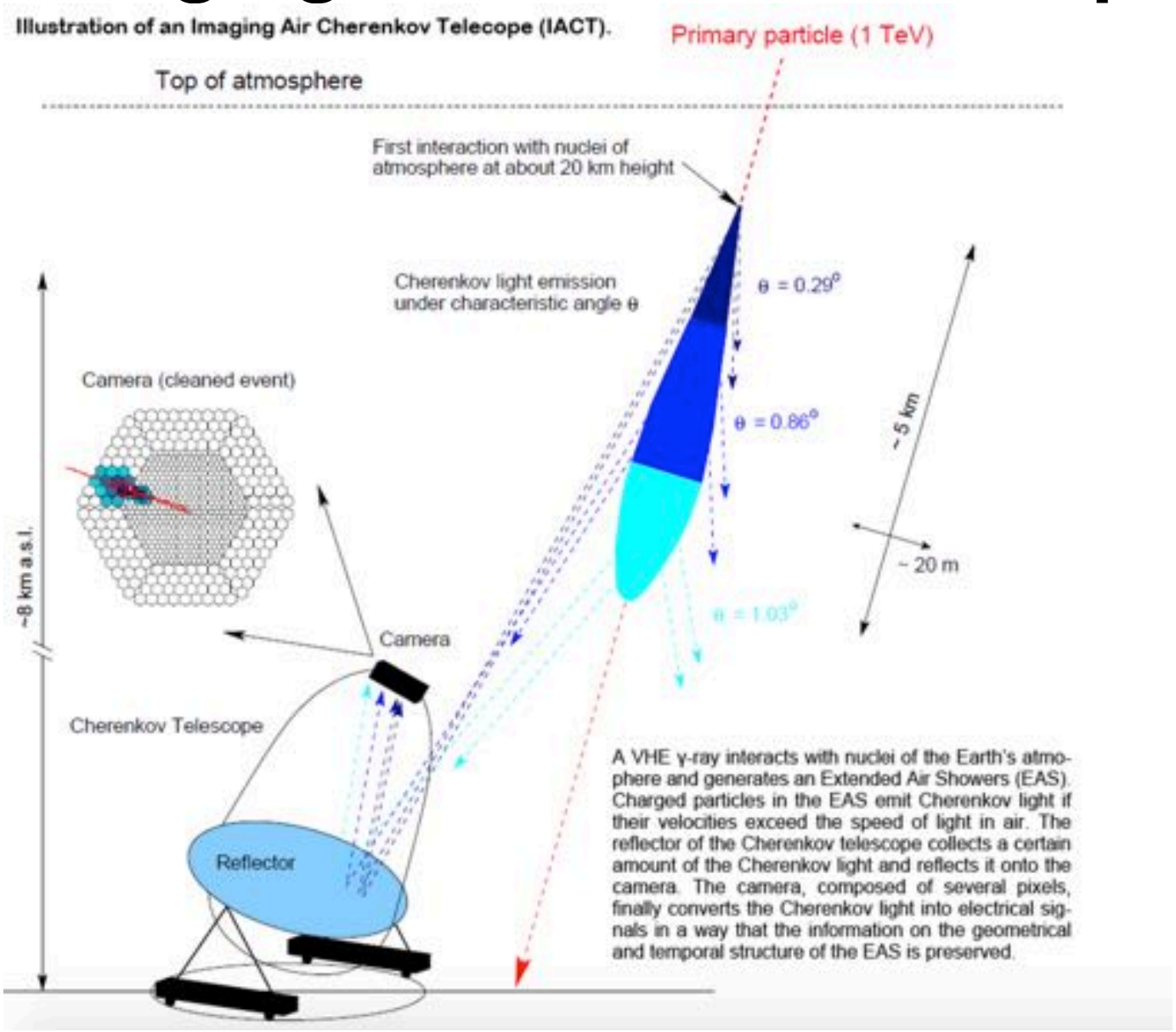

Fluorescence detector

- In addition to the direct detection of the shower components, it is interesting to measure indirectly to amount of particles in the shower.
- Fluorescence radiation:
  - High energy particles of the shower excite or ionize nitrogen molecules. N_2* de-excites in O(10) ns and emits isotropically near UV photons, with a yield of O(5~10) photons/m. The light yield is prop. to the number of charged particle at that height.
  - The shower profile can be observed from any direction, allowing to precisely reconstruct the shower profile development
  - Due to the small yield, only shower with $E>10^{18}$eV produce a measurable intensity of fluorescence light
  - Low duty cycle (only ~10/15%, during moonless nights)

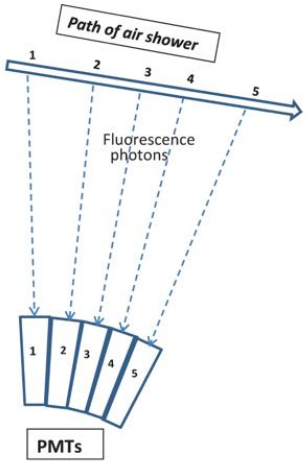

Fly's Eye technique (1981-1992)

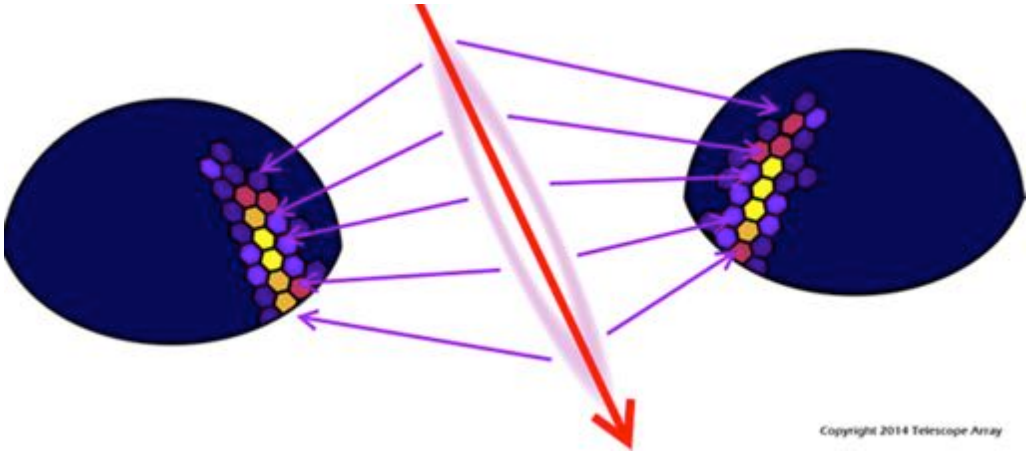

Fluorescence detector

- In addition to the direct detection of the shower components, it is interesting to measure indirectly to amount of particles in the shower.
- Fluorescence radiation:
  - High energy particles of the shower excite or ionize nitrogen molecules. N_2^* de-excites in O(10) ns and emits isotropically near UV photons, with a yield of O(5~10) photons/m. The light yield is prop. to the number of charged particle at that height.
  - The shower profile can be observed from any direction, allowing to precisely reconstruct the shower profile development
  - Due to the small yield, only shower with $E>10^{18}$eV produce a measurable intensity of fluorescence light
  - Low duty cycle (only ~10/15%, during moonless nights)

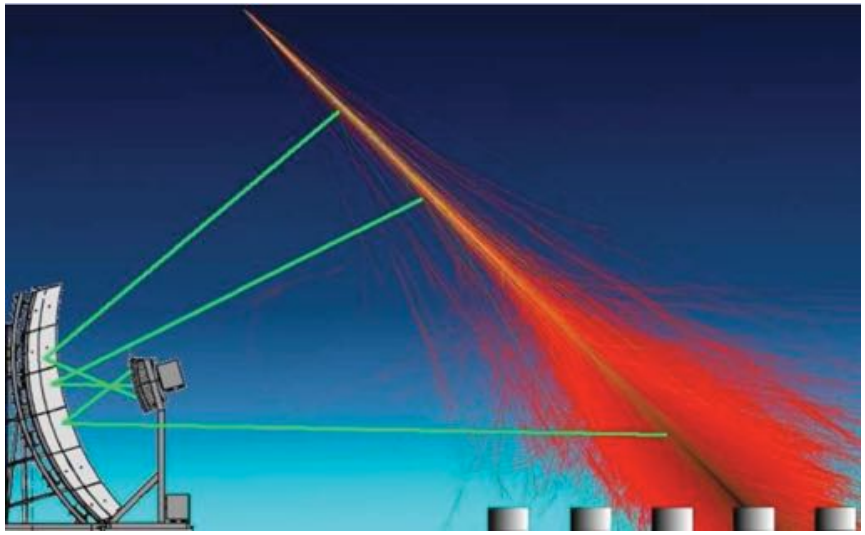

Hybrid detectors

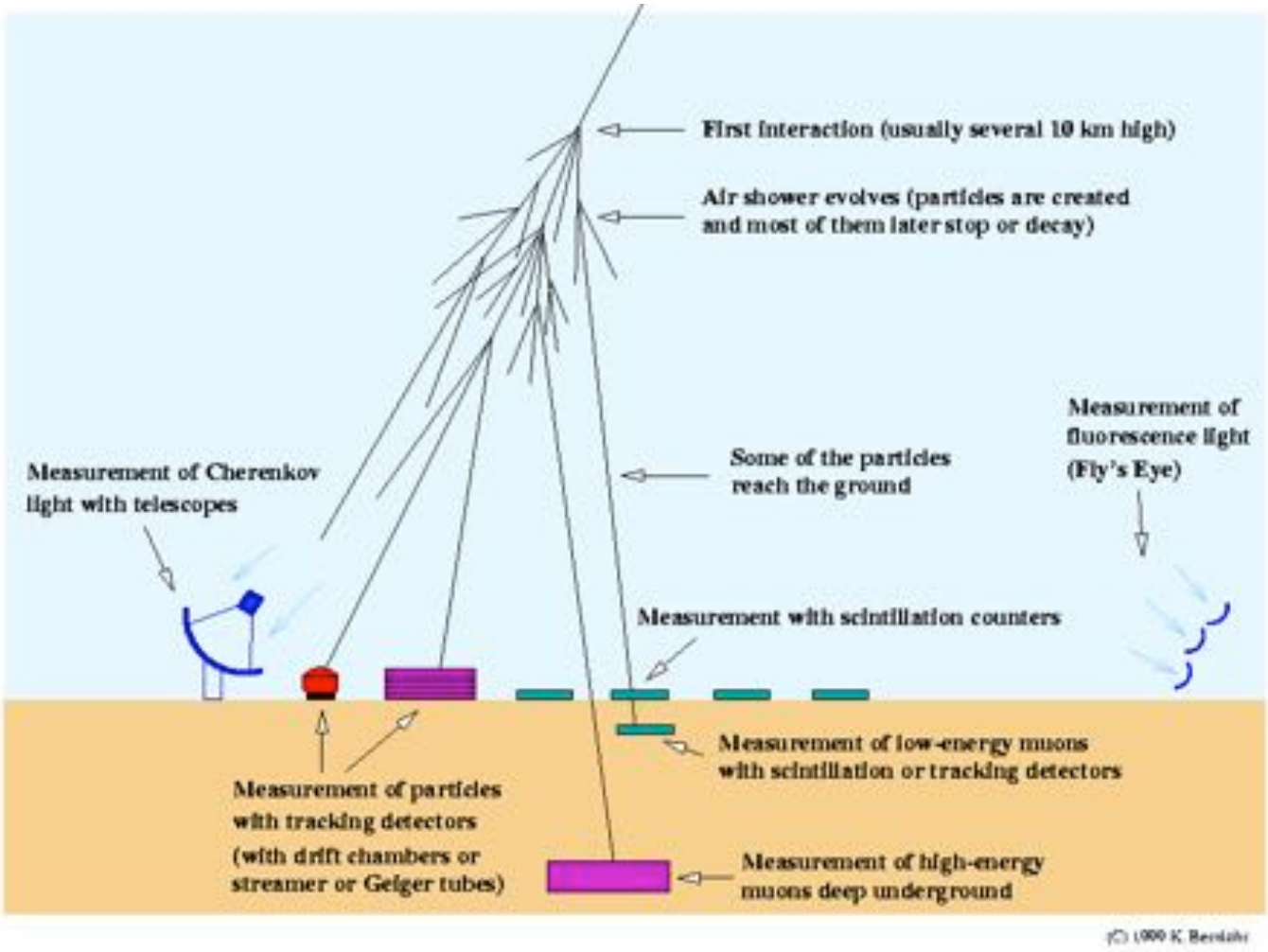

The primary cosmic ray characteristics are measured by higher sensitivities when the shower properties are measured by means of several techniques

Pierre Auger Observatory

The state-of-the-art extensive air shower detector is the Pierre Auger observatory

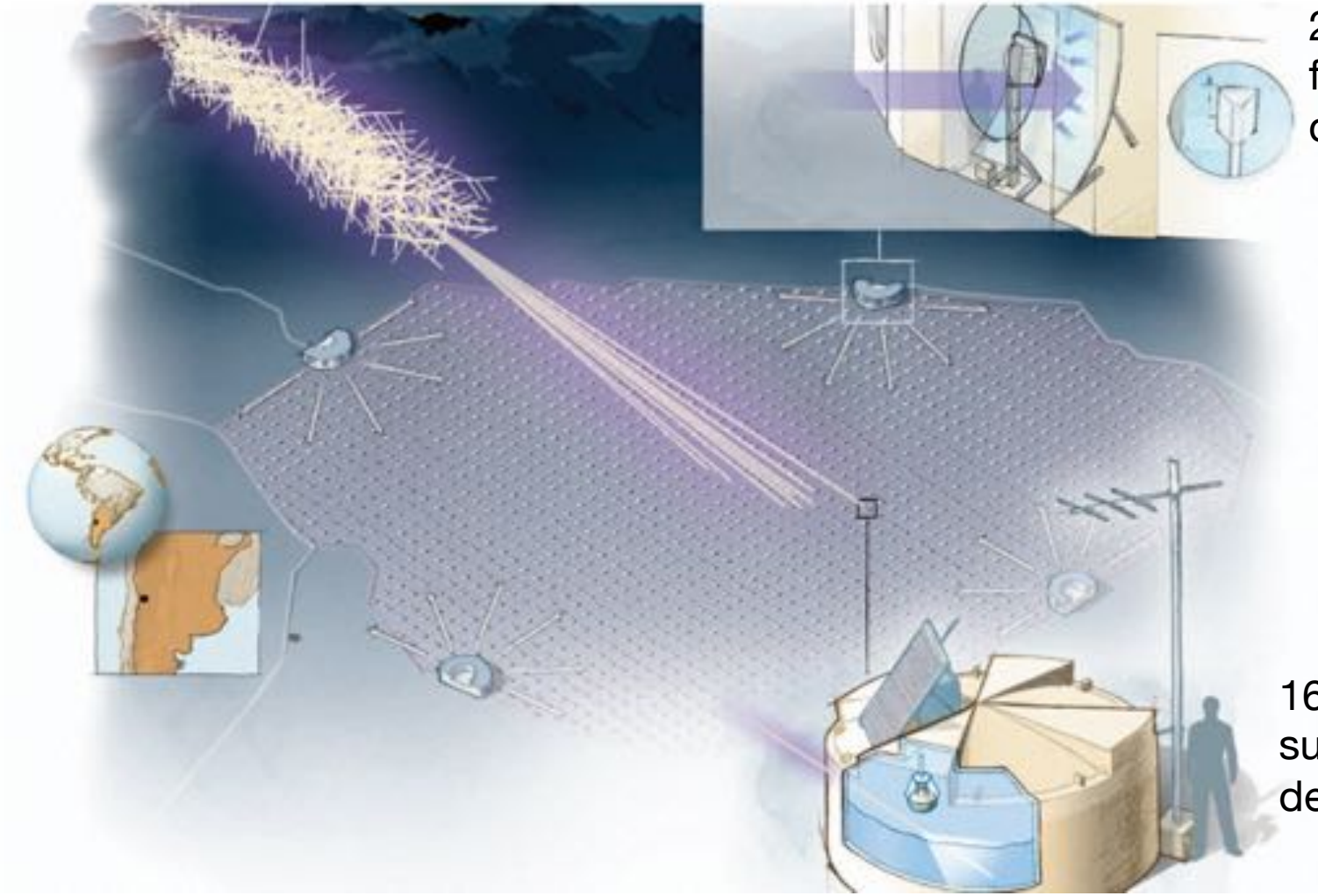

24 fluorescence detectors (FD)

1600 surface detectors (SD)

Pierre Auger Observatory

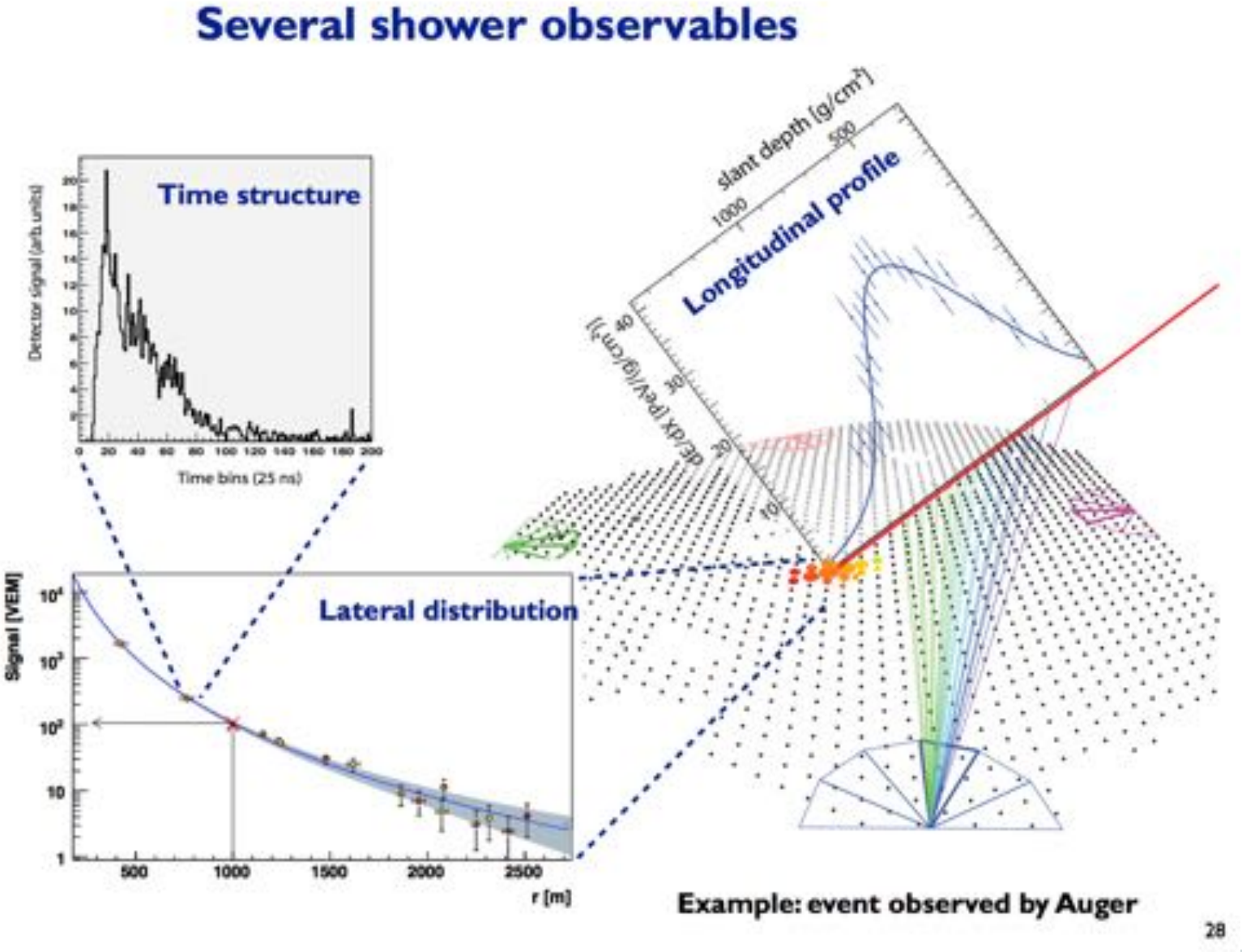

Pierre Auger Observatory

surface detectors LATERAL SPREAD	fluorescence detectors LONGITUDINAL PROFILE
⊕ 100% duty cycle	⊖ 10-15% duty cycle (clear, moonless nights)
⊕ acceptance = geometric	⊖ acceptance depends on distance and atmosphere
⊖ only last stage of shower development observed	⊕ full observation of longitudinal shower development
⊖ energy scale model dependent	⊕ (almost) model independent

→ combine two complementary techniques: Auger hybrid detector

Pierre Auger Observatory

The Surface Detector / SD

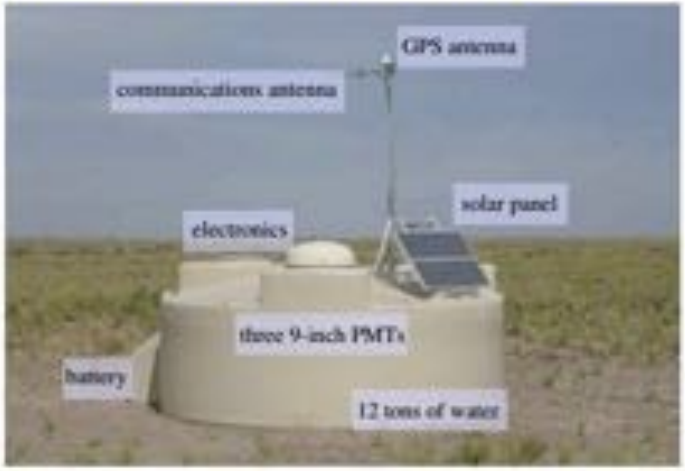

- 100% duty cycle
- full acceptance for $E \geq 3 \times 10^{18}$ eV

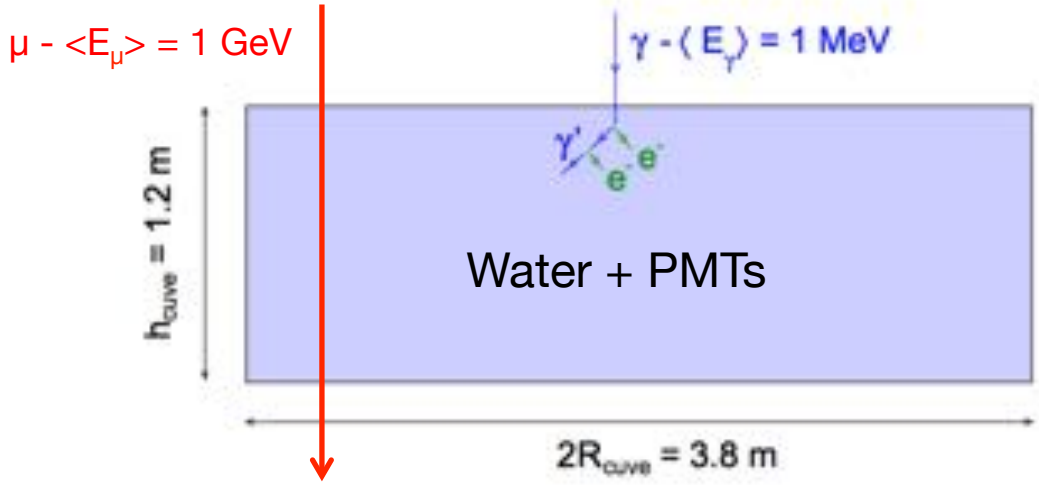

Muons at ground release much higher Cherenkov radiation than the EM component

Energy deposit expressed in Equivalen Vertical Muon
EVM = 240 MeV

Pierre Auger Observatory

Comparison of surface detectors

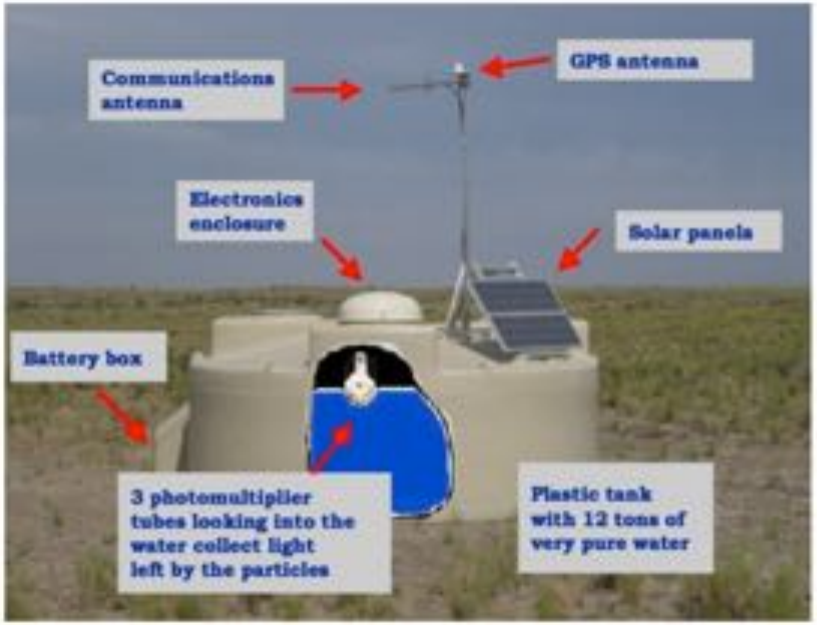

Auger: thick water-Cherenkov detectors
(large part of signal due to muons, large acceptance to inclined showers)

Telescope Array: thin scintillators
(main part of signal due to em. particles, low sensitivity to muons)

Complementary surface detector arrays

Pierre Auger Observatory

The Fluorescence Detector / FD

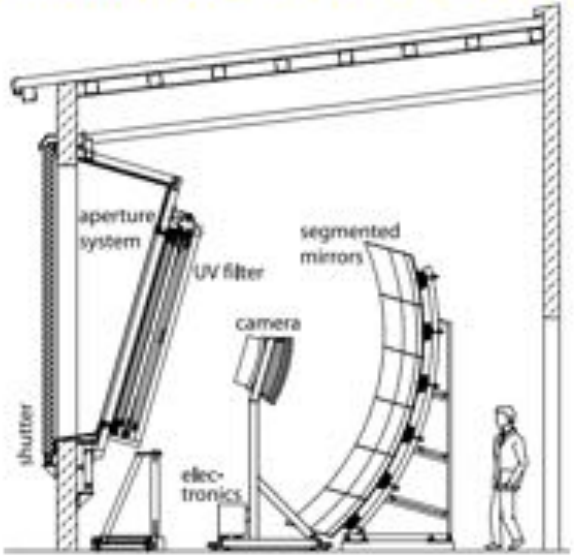

- 6 mirrors per building,
- each $30° \times 30°$ field of view,
- 440 PMT pixels per camera,
- UV filter.

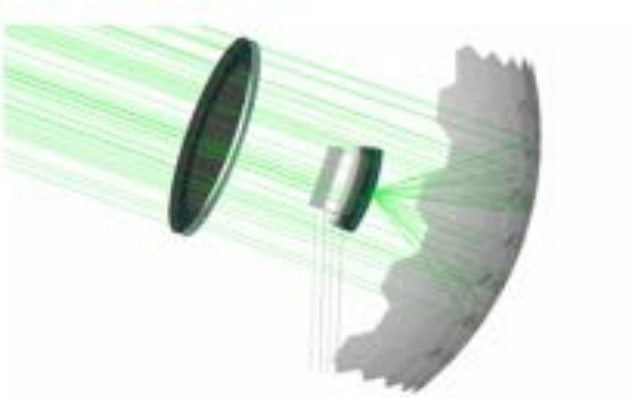

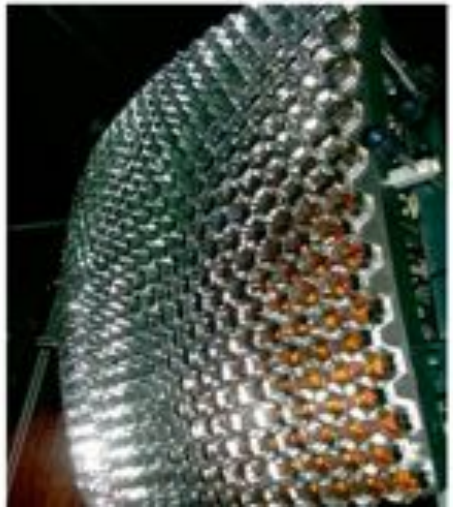

Pierre Auger Observatory

FD ⟶ Longitudinal profile

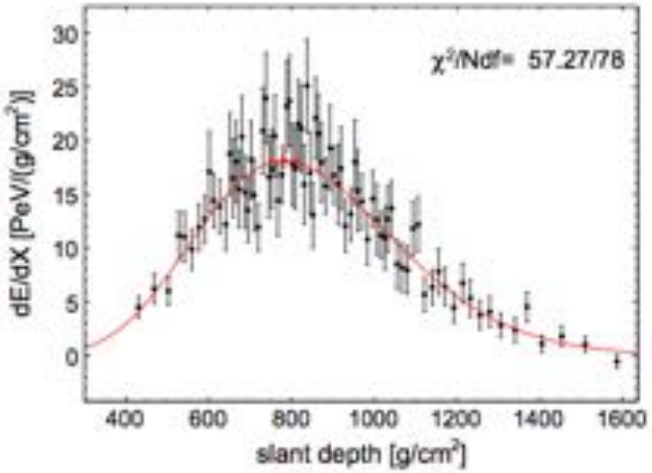

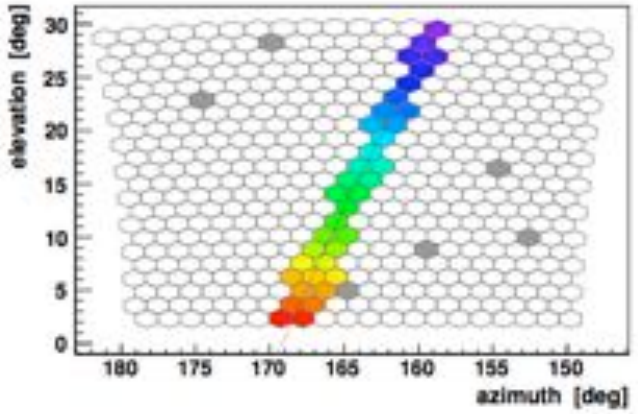

Longitudinal profile and mass composition

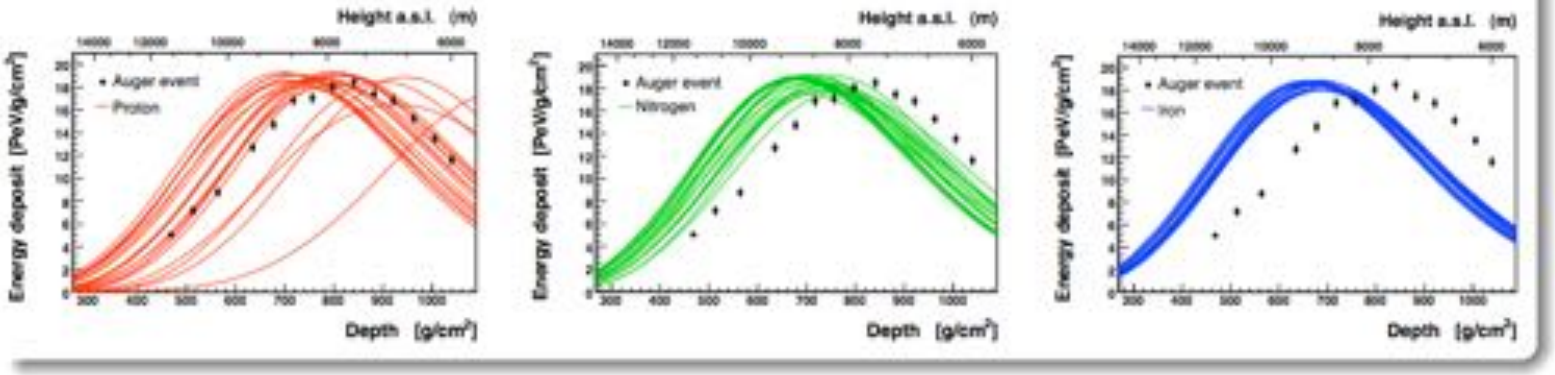

Pierre Auger Observatory

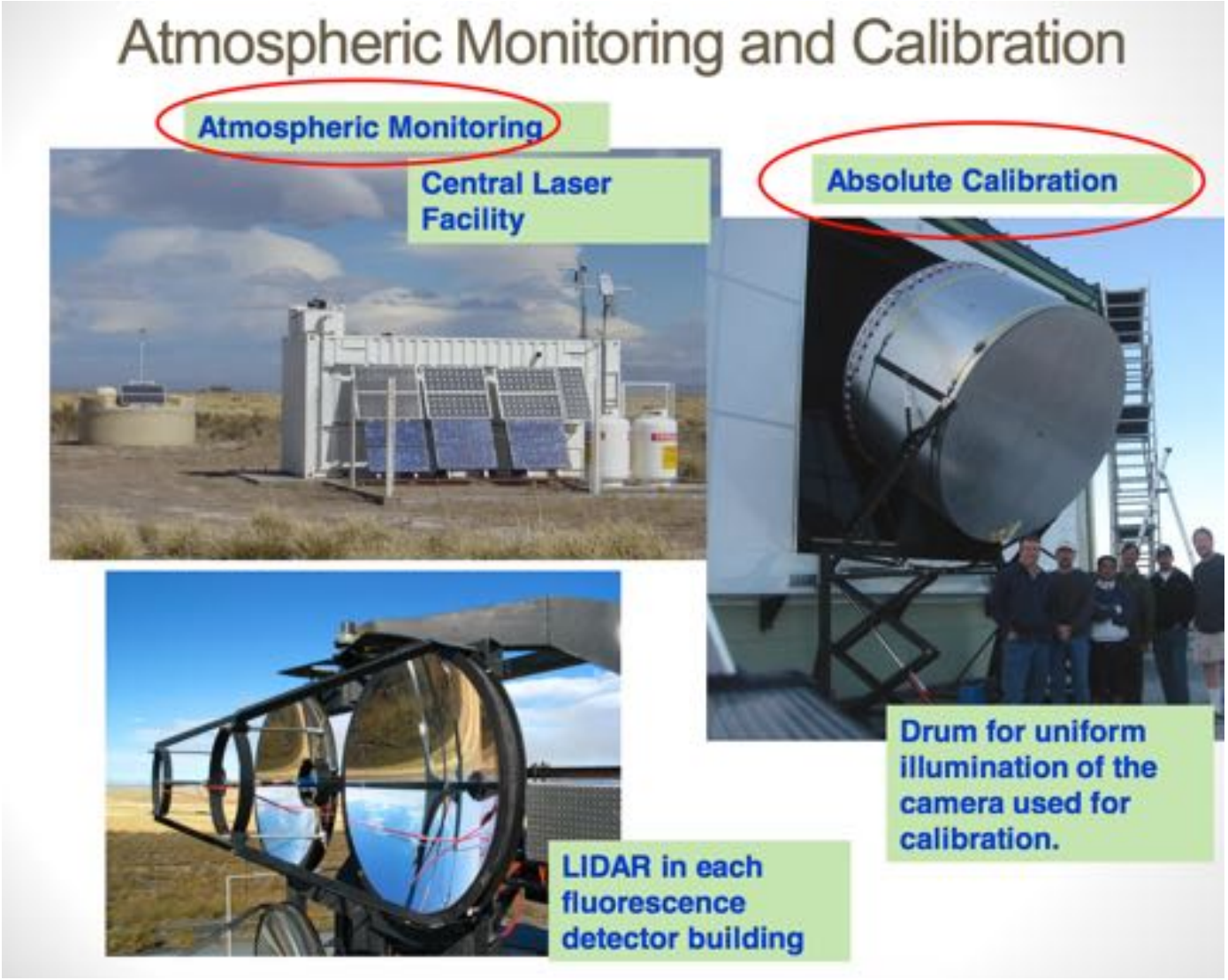

Pierre Auger Observatory

The hybrid technique allow to use the FD information to calibrate the energy deposits measured by the SD

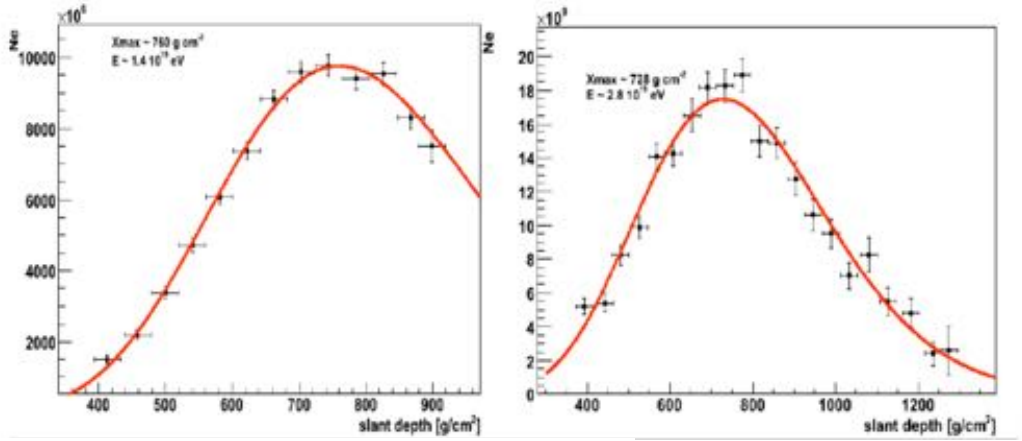

Calorimetric measurement of the energy (FD)

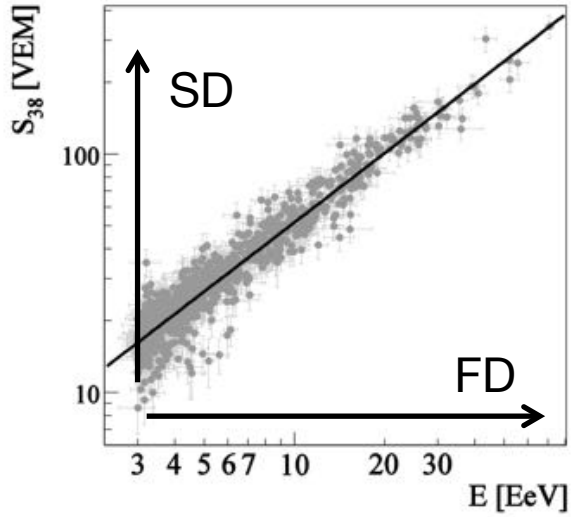

Calibration of SD measurement with hybrid events

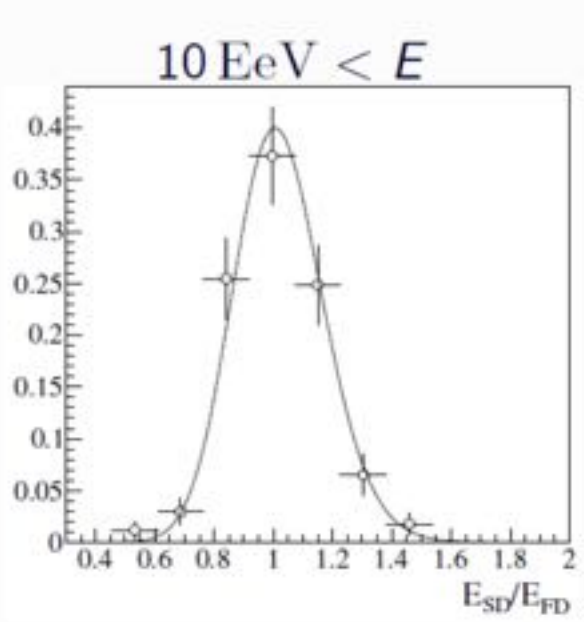

$\sigma_{SD}/E_{SD} = (12 \pm 1)\%$

Pierre Auger Observatory

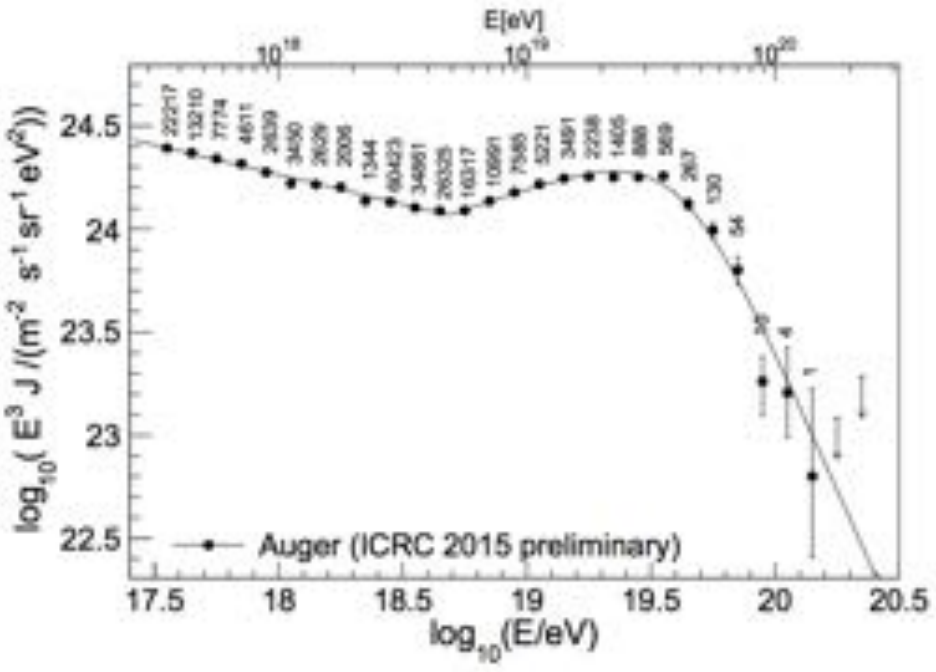

Figure 3: The combined energy spectrum of cosmic-rays as measured by the Auger Observatory, fitted with a flux model (see text). Only statistical uncertainties are shown. The systematic uncertainty on the energy scale is 14%. The number of events is given above the points, which are positioned at the mean value of $\log_{10}(E/\text{eV})$. The upper limits correspond to the 84% C.L.

The data show a sharp cutoff at energies above 10^{20}eV, as predicted by the GZK mechanism. However, this would imply that most of UHECRs are protons (the GZK energy threshold for nuclei is above that of protons)

Pierre Auger Observatory

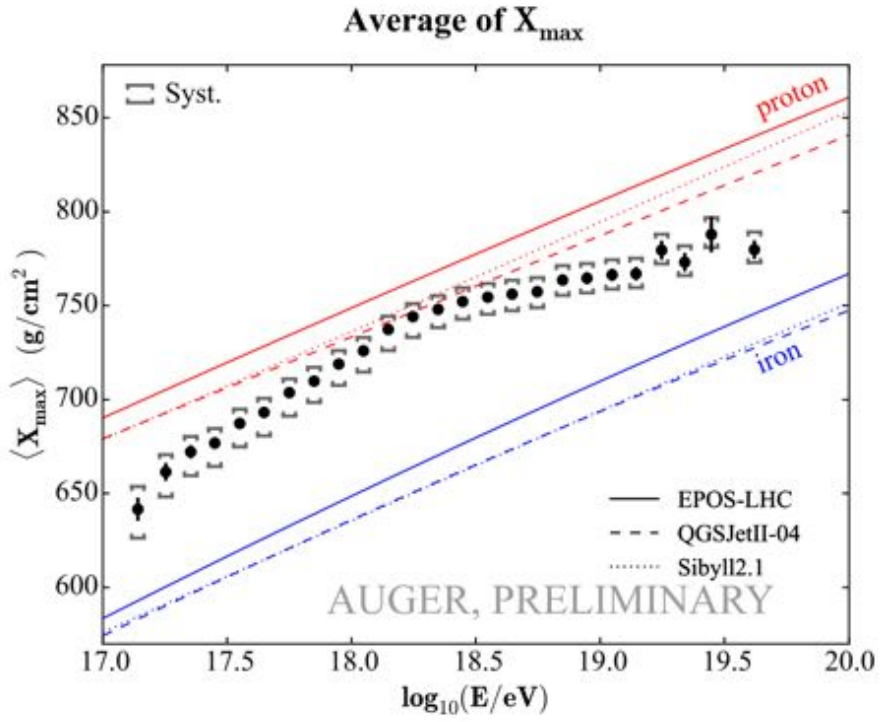

Events are not discriminated on event-by-event basis, but only through statistical inference from the total collected sample.
Xmax provides information on the mass number of the primary nuclei. Auger results show a trend towards a high-mass composition above the ankle.

Pierre Auger Observatory

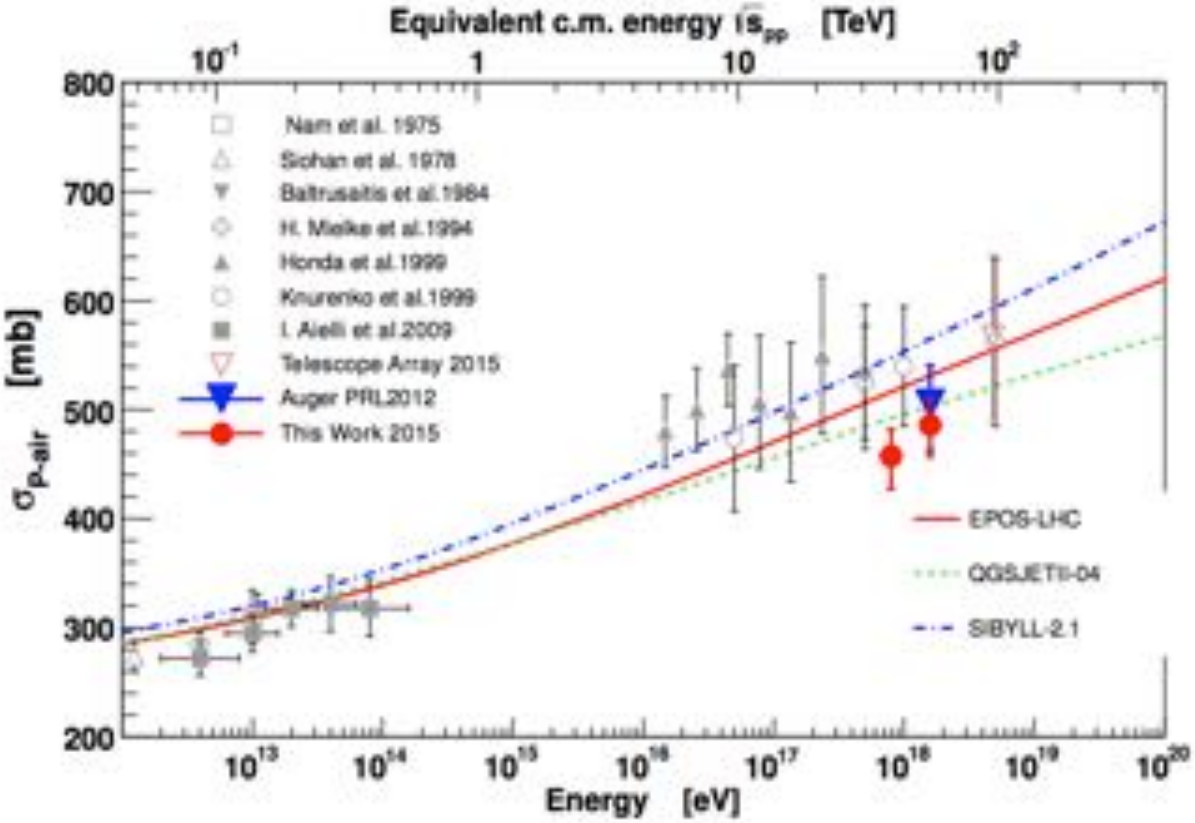

- Measurements at EAS are also used to extend cross-sections measurements at energies above the laboratory reach
- Such measurements are fundamental to test and verify the prediction of the hadronic interaction models

Imaging Air Cherenkov Telescopes

- Imaging Air Cherenkov Telescopes (IACTs) are primarly used to detect electromagnetic cascades initiated by high energy gamma-rays and $e^{+/-}$
- Imaging: the Cherenkov light is focused in a multi-pixel camera to reconstruct the shower properties

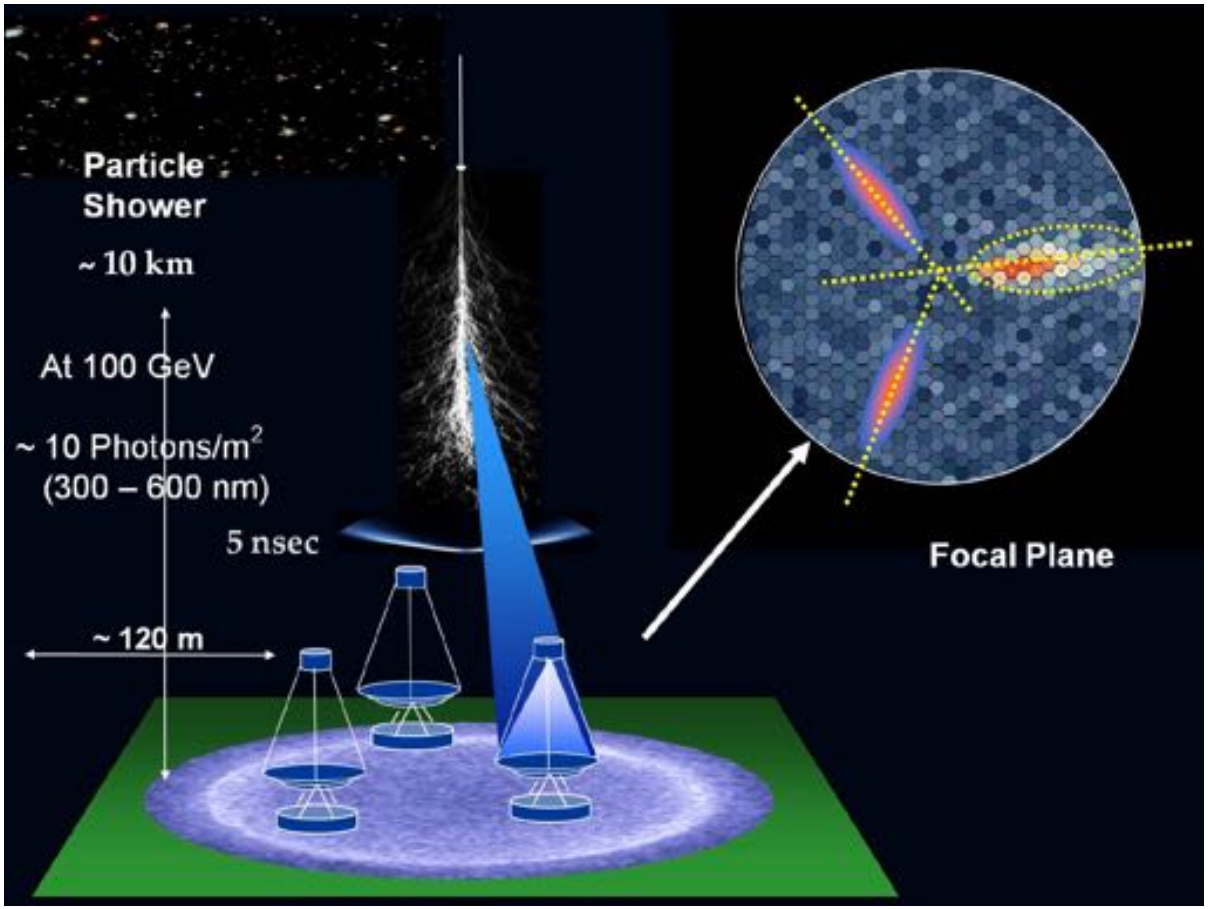

Imaging Air Cherenkov Telescopes

- The Cherenkov angle increases with the refractive index (more specifically with n-1, will revisit this later.)

- Water ≈ 41°
- Air ≈ 1.0 to 1.3°

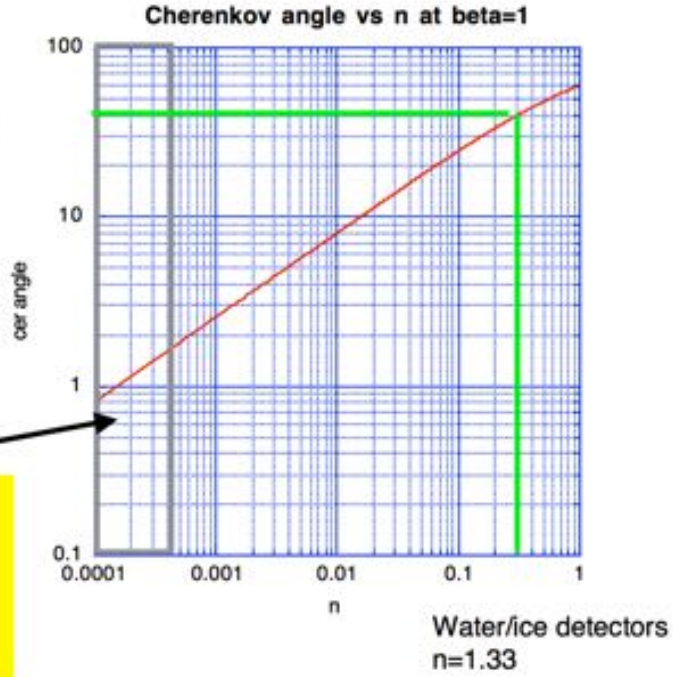

Water/ice detectors
n=1.33

Atmosphere:
Increasing density down to sea level (n=1.0003)

→Changing Cherenkov angle
→Unique optics

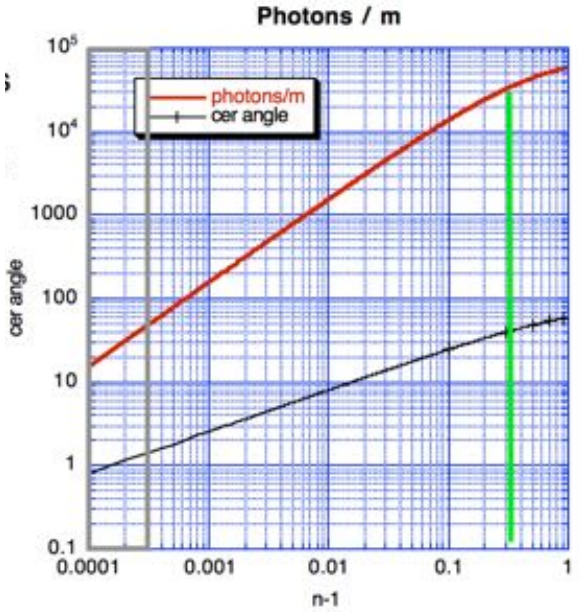

- Number of Cherenkov photons for β=1 particles as function of the refractive index, or more precisely of (n-1).
- Integrated from ≈400 to 700 nm.

Threshold energy for electrons:

- Air: 20 MeV
- Water/ice: 0.7 MeV

Imaging Air Cherenkov Telescopes

NIGHT SKY BACKGROUND

- Moon
- Airglow
  - the brightest component and is caused by oxygen atoms glowing in the upper atmosphere which are excited by solar ultraviolet radiation. Airglow gets worse at solar maximum. (increases towards red)
- Zodiacal light
  - Interplanetary dust particles reflect and scatter sunlight and make up the zodiacal light and gegenschein (increases towards red)
- Star light
  - Stars mostly from Milky way
  - includes starlight is scattered by the atmosphere, just as sunlight is during the daytime. (Slightly blue)
- Aurorae borealis:
  - Cosmic ray particles from solar wind cause glow in upper atmosphere; mostly in polar regions where they spiral down the magnetic poles.

- Moonless night sky total background: $\approx 10^{12}$ photons/(m^2s sr) (± factor ≈2)

Imaging Air Cherenkov Telescopes

- Night sky background: $\phi_{NSB} = 10^{12}$ photons/(m^2 s sr)
- Cherenkov pulse: $\phi_{Ch} = 10$ photons/m^2/3ns
- Transmittance of atmosphere
- qE=quantum efficiency
- Instruments: PMT, mirrors, electronics
- Number of signal photoelectrons: $\phi_{Ch} * A * T * qE$
- Number of background photoelectrons: $\phi_{NSB} * A * T * qE * \tau * \Omega$
- Solid angle greater than shower (> 1 degree)

$$\frac{Signal}{Noise} = N_\sigma = \frac{\Phi_{ch} \cdot A \cdot T \cdot qE}{\sqrt{\Phi_{NSB} \cdot A \cdot \Omega \cdot T \cdot qE \cdot \tau}}$$

$$N_\sigma = \Phi_{ch} \sqrt{\frac{T \cdot A \cdot qE}{\Phi_{NSB} \cdot \Omega \cdot \tau}}$$

To achieve a reasonable S/N, detector, we have to tune A and Ω.
The solution involves the pixelation of the camera (small Ω per channel), with the possibility to trigger the event only if an interesting pattern of fired pixel is measured in the camera

Imaging Air Cherenkov Telescopes

- IACTs provide improved sensitivity in the high energy range, where the sensitivity of space borne detectors is limited by their low acceptance

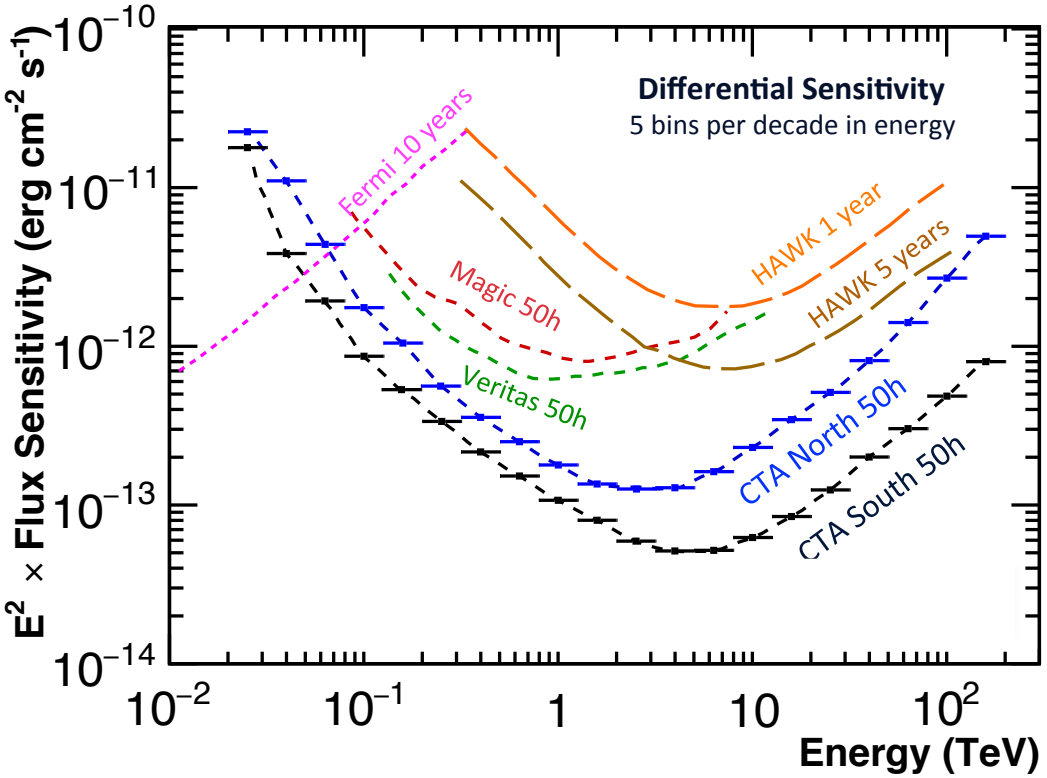

Imaging Air Cherenkov Telescopes

- Imaging reconstruction allows to separate the interesting EM signal from the background hadronic shower or muon rings

MONO observation mode

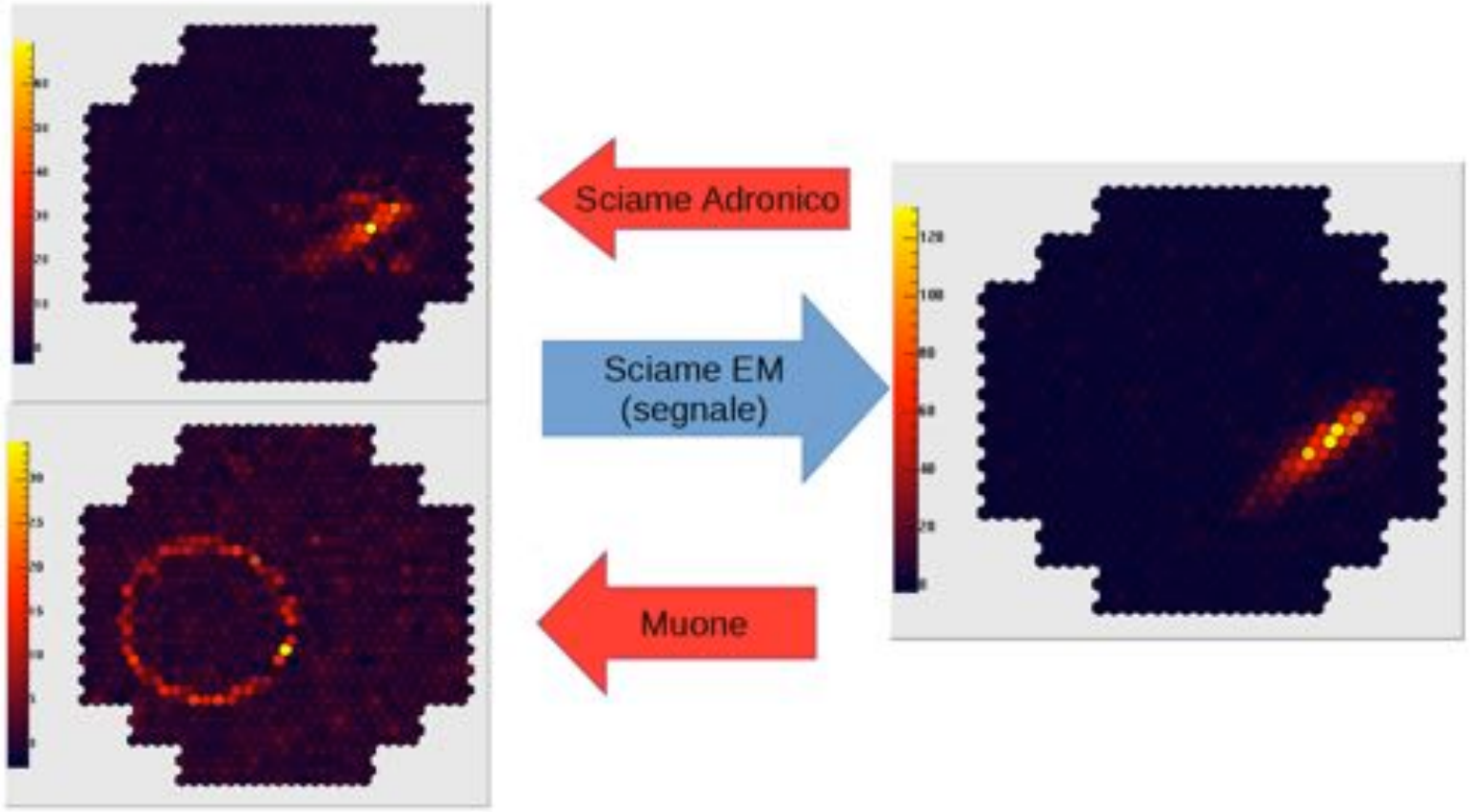

Imaging Air Cherenkov Telescopes

- Imaging reconstruction allows to separate the interesting EM signal from the background hadronic shower or muon rings

STEREO observation mode

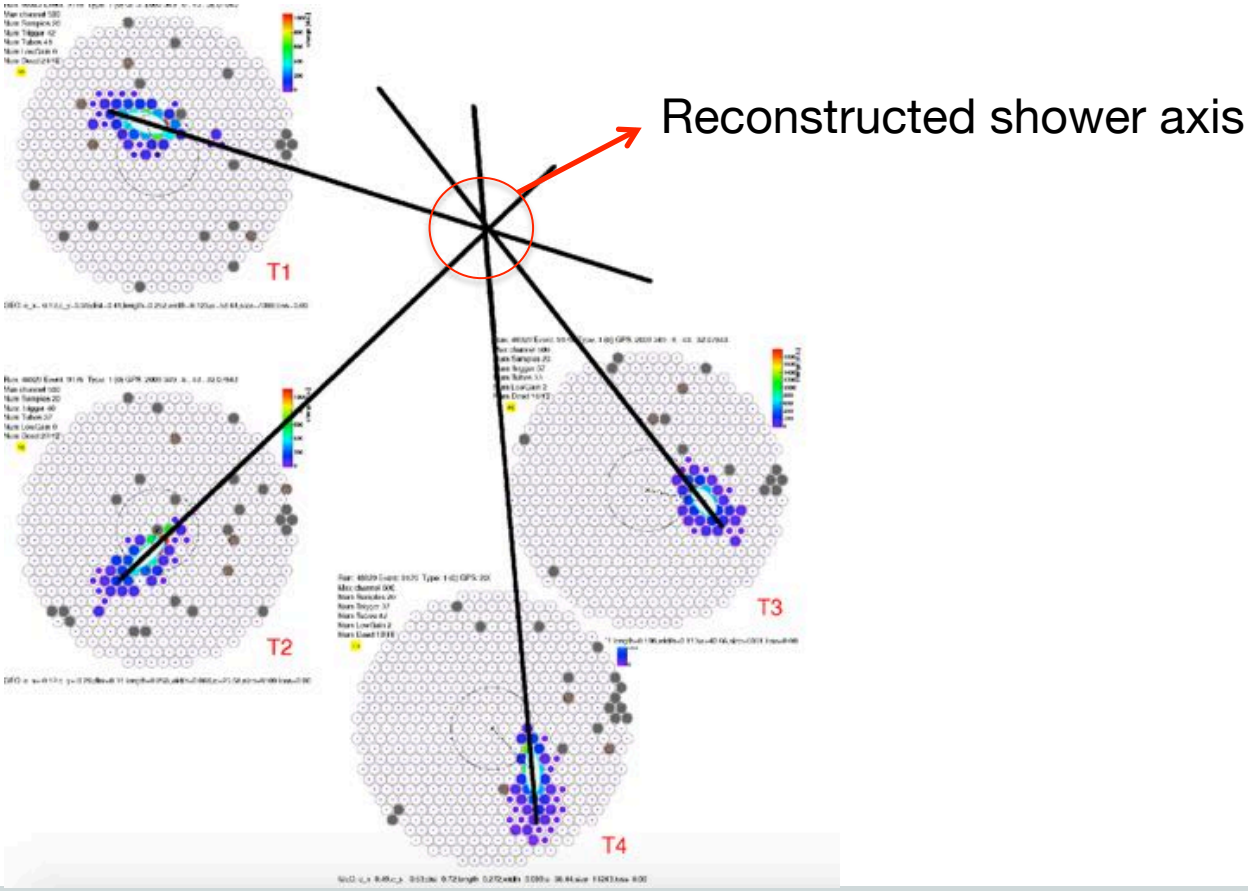

Imaging Air Cherenkov Telescopes

- Imaging reconstruction allows to separate the interesting EM signal from the background hadronic shower or muon rings

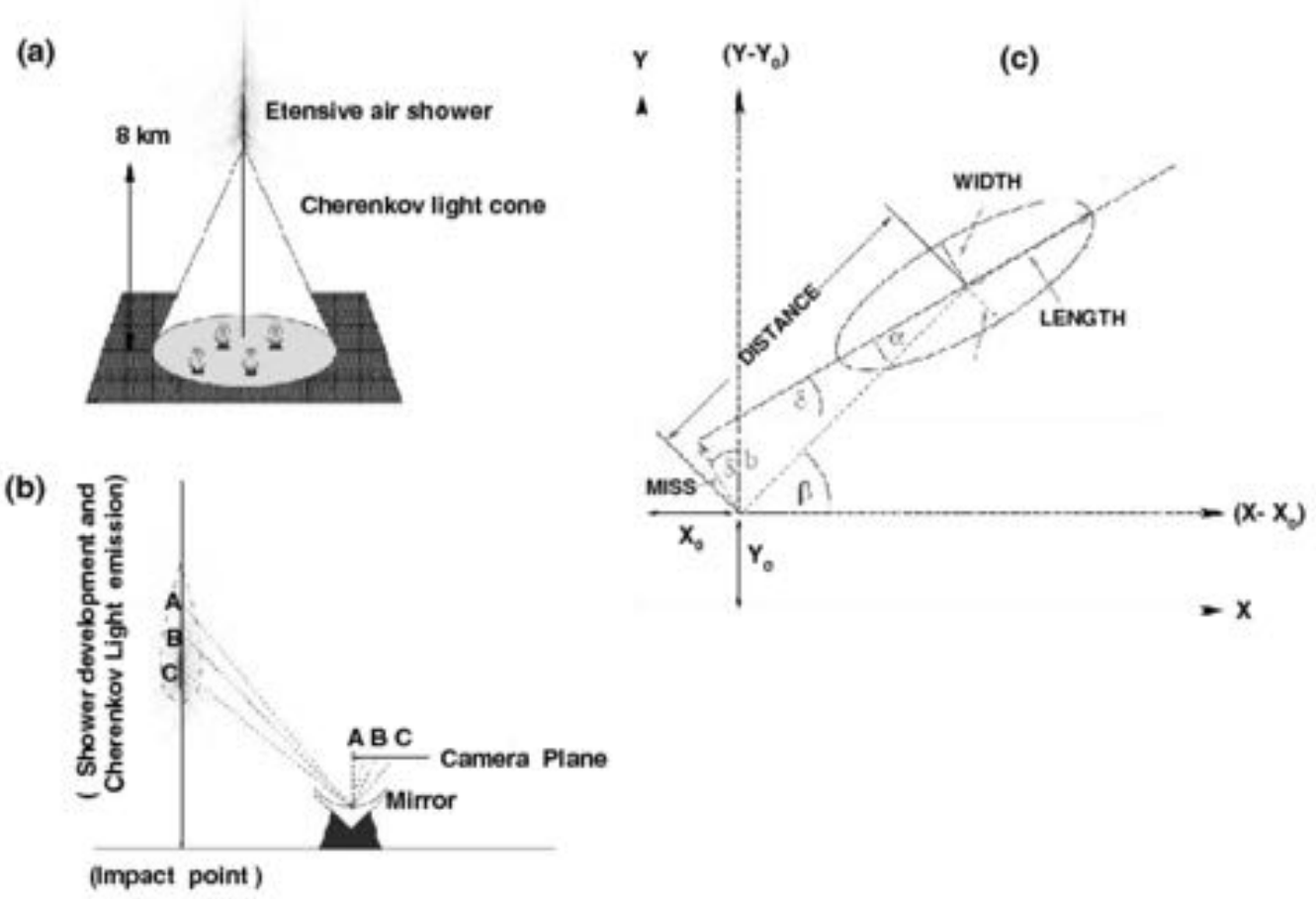

The current IACT generation

H.E.S.S. (Namibia)

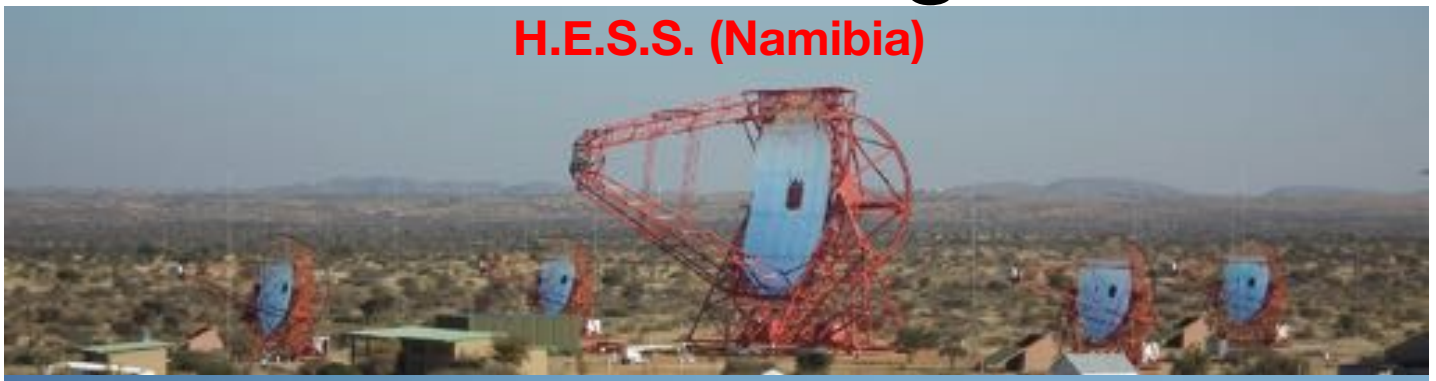

VERITAS (Arizona)

MAGIC (La Palma)

Performances:

- Sensitive to primary photons in the 100 GeV – 10 TeV energy range
- Energy resolution ~20%
- Duty cicles < 15%
- Angular resolution ~ 0.1° at high energies

The Cameras

The HESS II camera

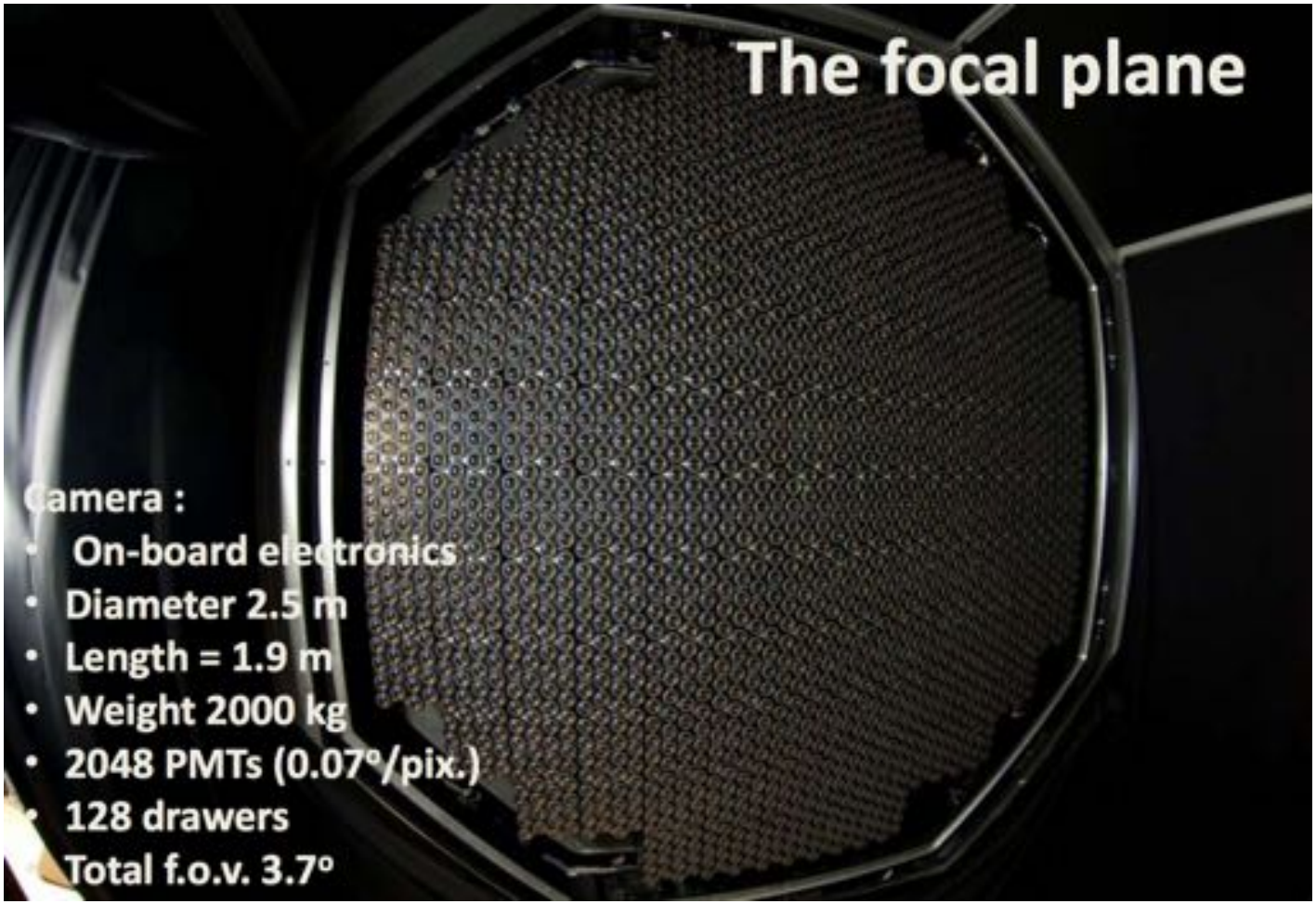

PMTs with a maximum Photon Detection Efficiency of 30%

High energy gamma-ray science

- The science targeted by IACTs is very variegate, and it involves many topics of astrophysics and particle physics
- I will mention few, which are more “particle-physics” related
- The field is wide, you can look up yourself if you are interested in the topics that I will not cover

HESS galactic sky survey

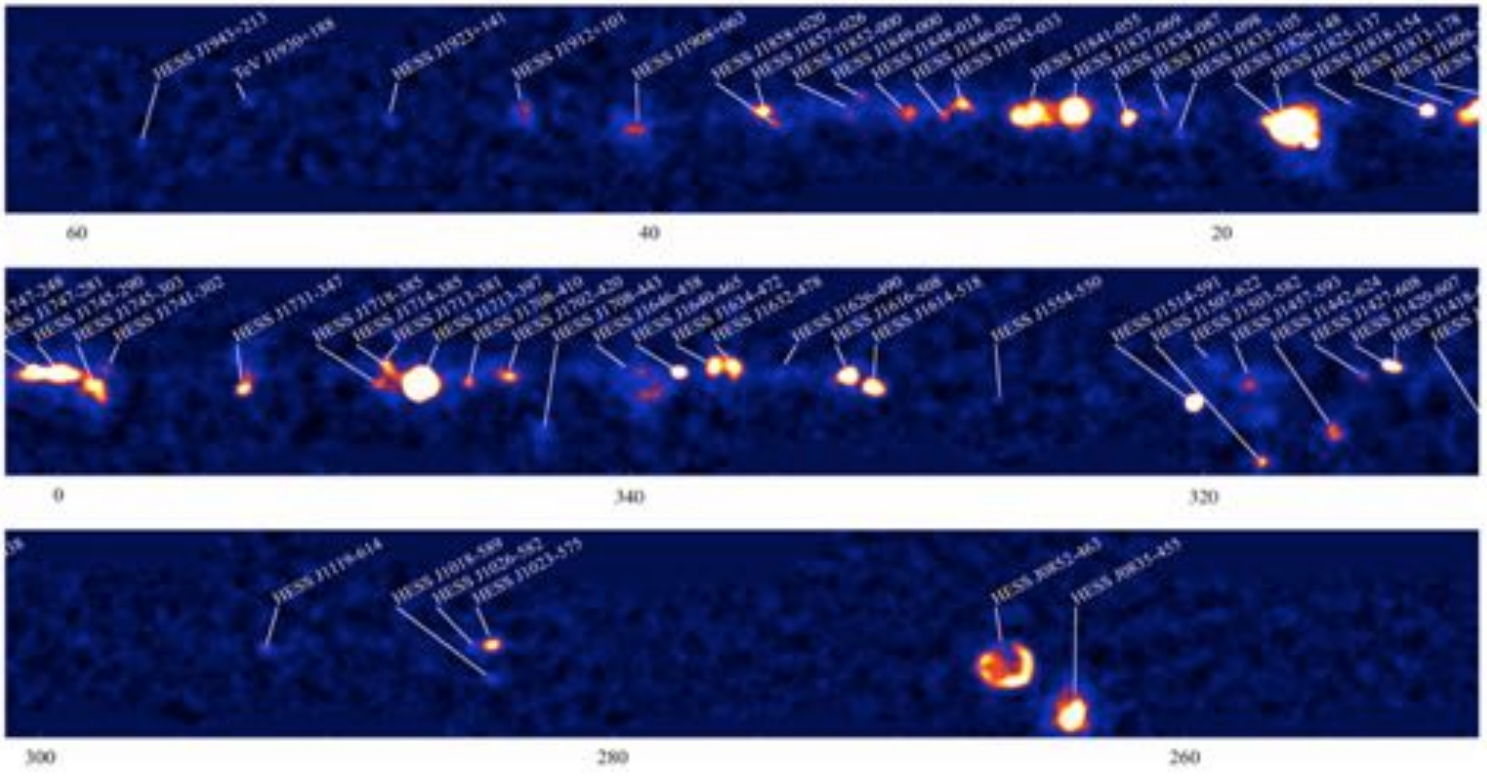

High energy gamma-ray science

Cosmic Ray Acceleration Mechanisms

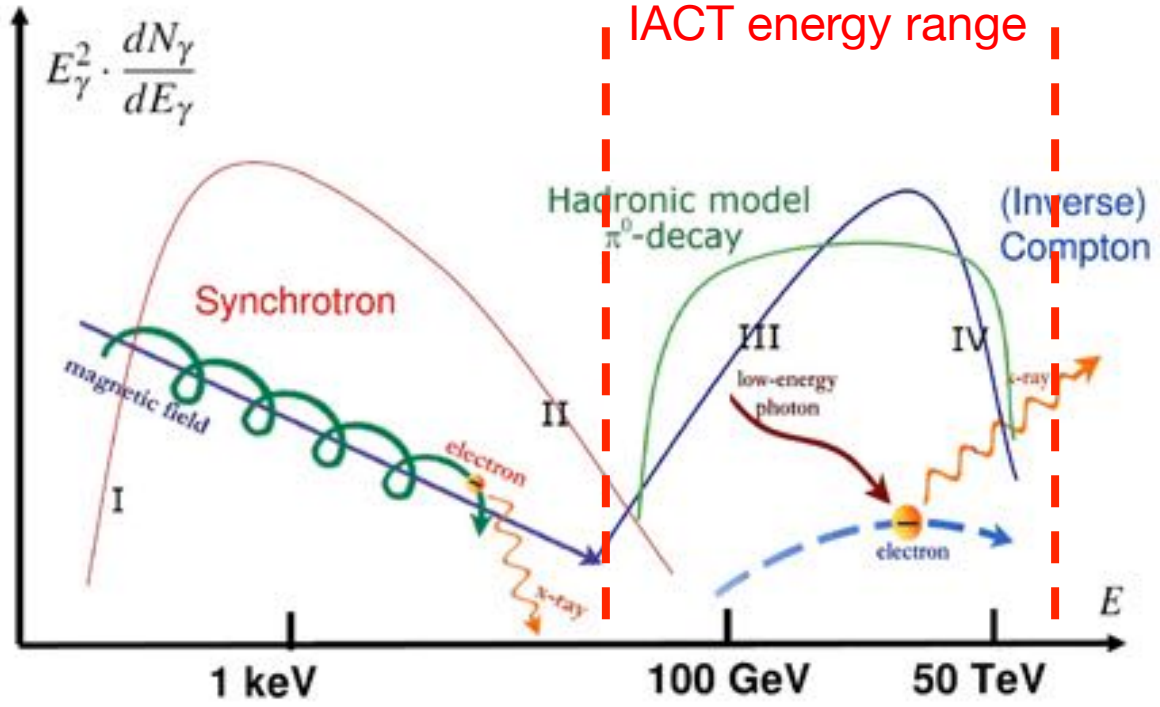

Fig. 8.1. Spectral energy distribution of photons produced in leptonic/hadronic models. Synchrotron radiation is caused by relativistic electrons accelerated in a magnetic field. Photons from synchrotron emission represent also the target for inverse Compton scattering of the parent electrons. When hadrons interact with matter or ambient photons, a distribution of γ-rays from π^0 decays as indicated by the green curve could be obtained. Superimposition of γ-rays from both leptonic and hadronic mechanisms is assumed in case of mixed models. Adapted

High energy gamma-ray science

Spectral and morphological studies of CR sources

γ-ray spectrum of RX J1713.7-3946 compared with expectations for lepton CR rigin models. The same spectrum cannot however rule out the hadronic hypothesis in presence of a hard injection spectrum

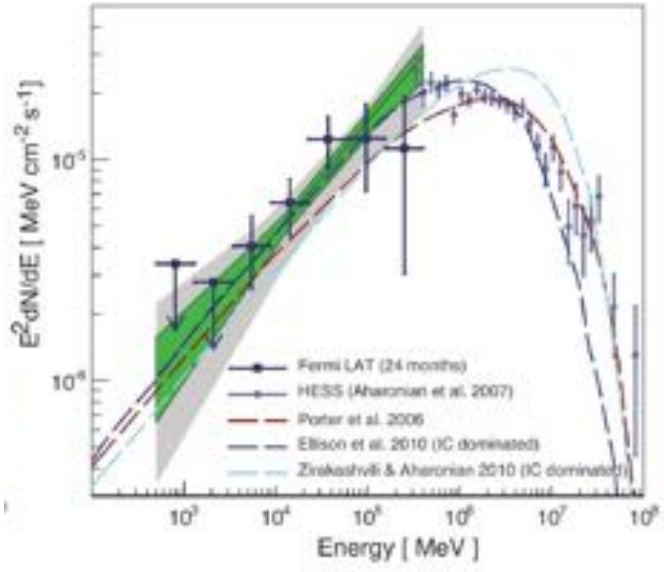

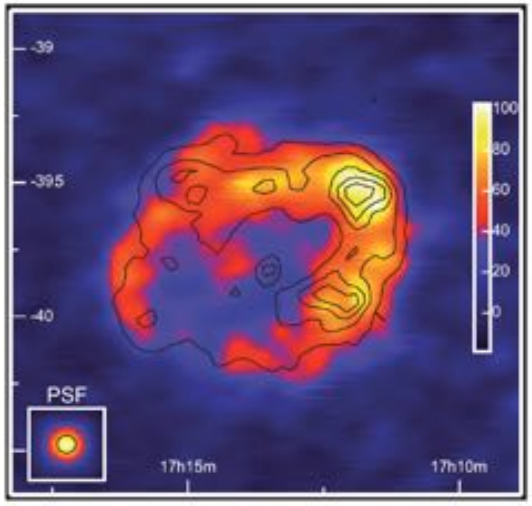

Fig. 9.11. HESS map of γ-ray excess events for RX J1713.7-3946 - the first SNR shell to be resolved at TeV energies. The superimposed contours show the *X*-ray surface brightness as seen by ASCA in the 1-3 keV range. On the bottom left, the HESS point spread function

The detailed morphological studies possible with IACTs at the level of 0.1° shows that the acceleration sites are spatially coincident with the sites of non-thermal X -ray emission, strengthening the hypothesis that primary galactic CRs up to the “knee” are accelerated in SNRs. The identification of these objects is still an open field

High energy gamma-ray science

Dark Matter indirect searches

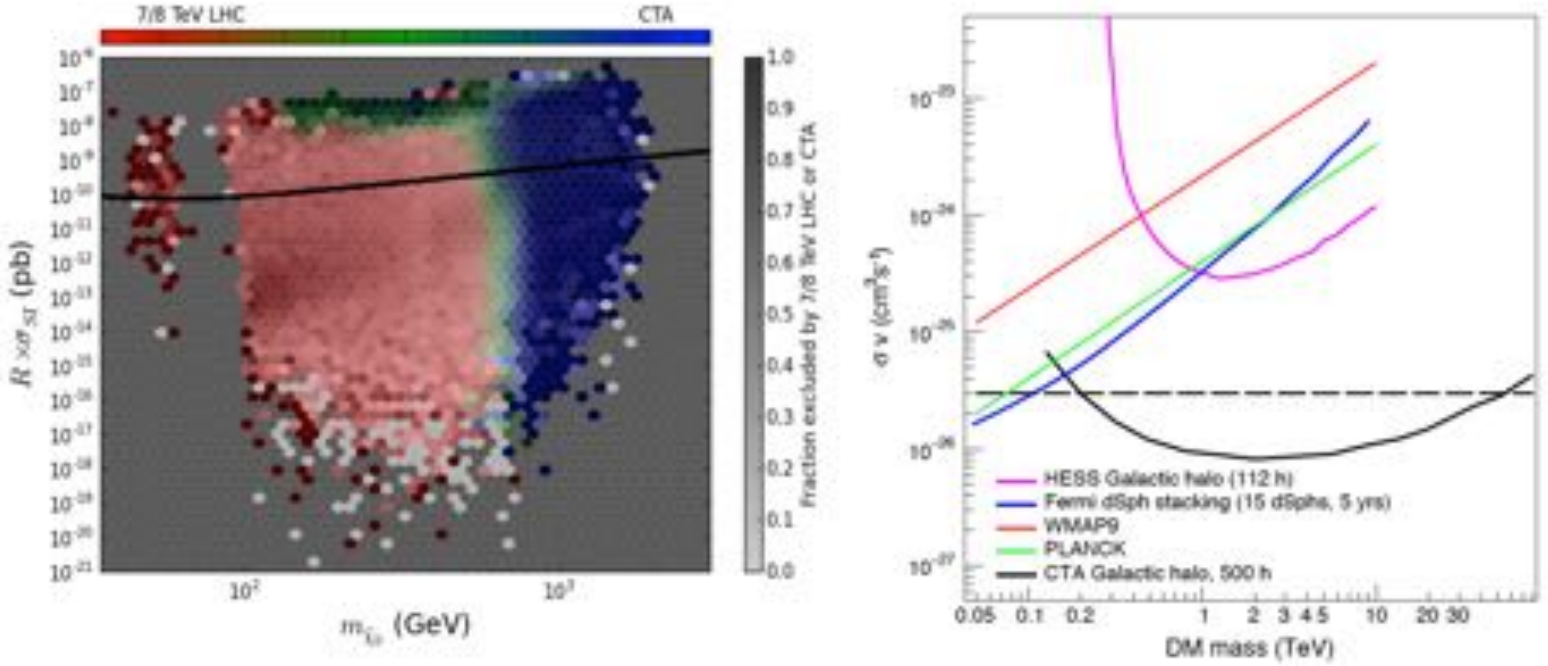

Figure 4.3 – Left: Comparisons of models from the phenomenological minimal supersymmetric model (pMSSM) surviving or being excluded by future direct-detection, indirect-detection and collider searches in the neutralino mass-scaled spin-independent cross section plane. The spin-independent XENON1T exclusion is shown as a solid black line. Figure extracted from [74]. Left: Current best limits on the annihilation cross section from indirect detection (Fermi-LAT and H.E.S.S.) and cosmic microwave background (WMAP and Planck) experiments [52]. Also shown is the projected sensitivity for CTA from observations of the Galactic halo.

High energy gamma-ray science

Electron + Positron spectrum

- IACTs cannot distinguish between photon-initiated showers and electron/positron initiated showers
- e+/- are identified as EM showers when pointing out of gamma-ray sources (photons keep directionality, e+/- are ~isotropic)
- Complementarity with space born experiments: extension of spectra at higher energies (but worst accuracy due to energy scale uncertainty and hadronic and gamma-ray background)

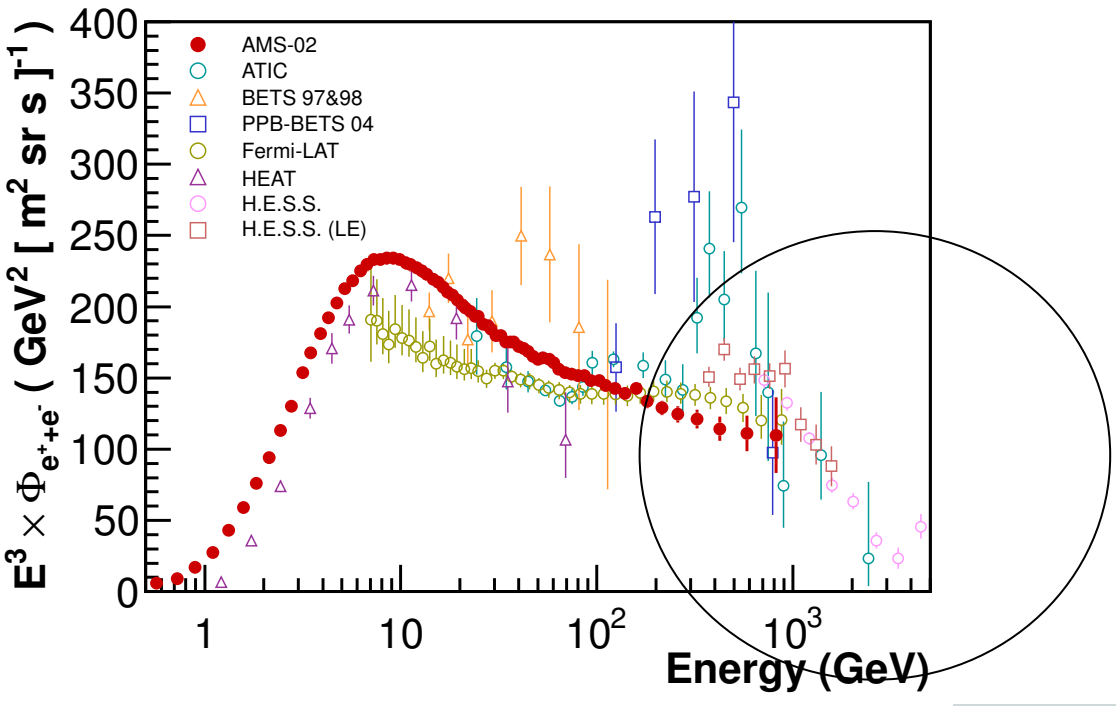

Cutoff at high energies observed by ground telescopes above 1 TeV

The next IACT generation

- **The Cherenkov Telescope Array** is a project that intends to improve the current IACT telescope sensitivities and extend the maximum energy range up to 100 TeV photons.
- To achieve this target, the community efforts are focused towards a unique, global project that intends to build two arrays of telescopes, one in the northern emisphere and one in the southern emisphere, to achieve a complete coverage of the sky.

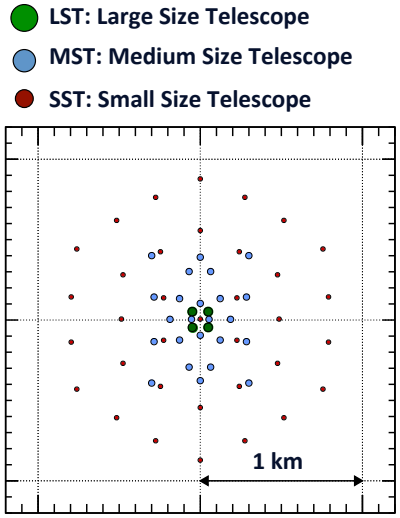

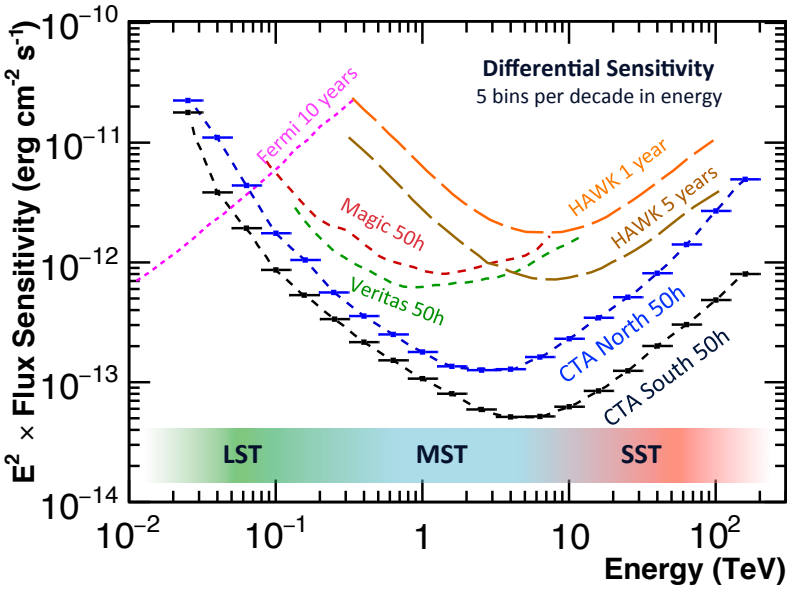

The next IACT generation

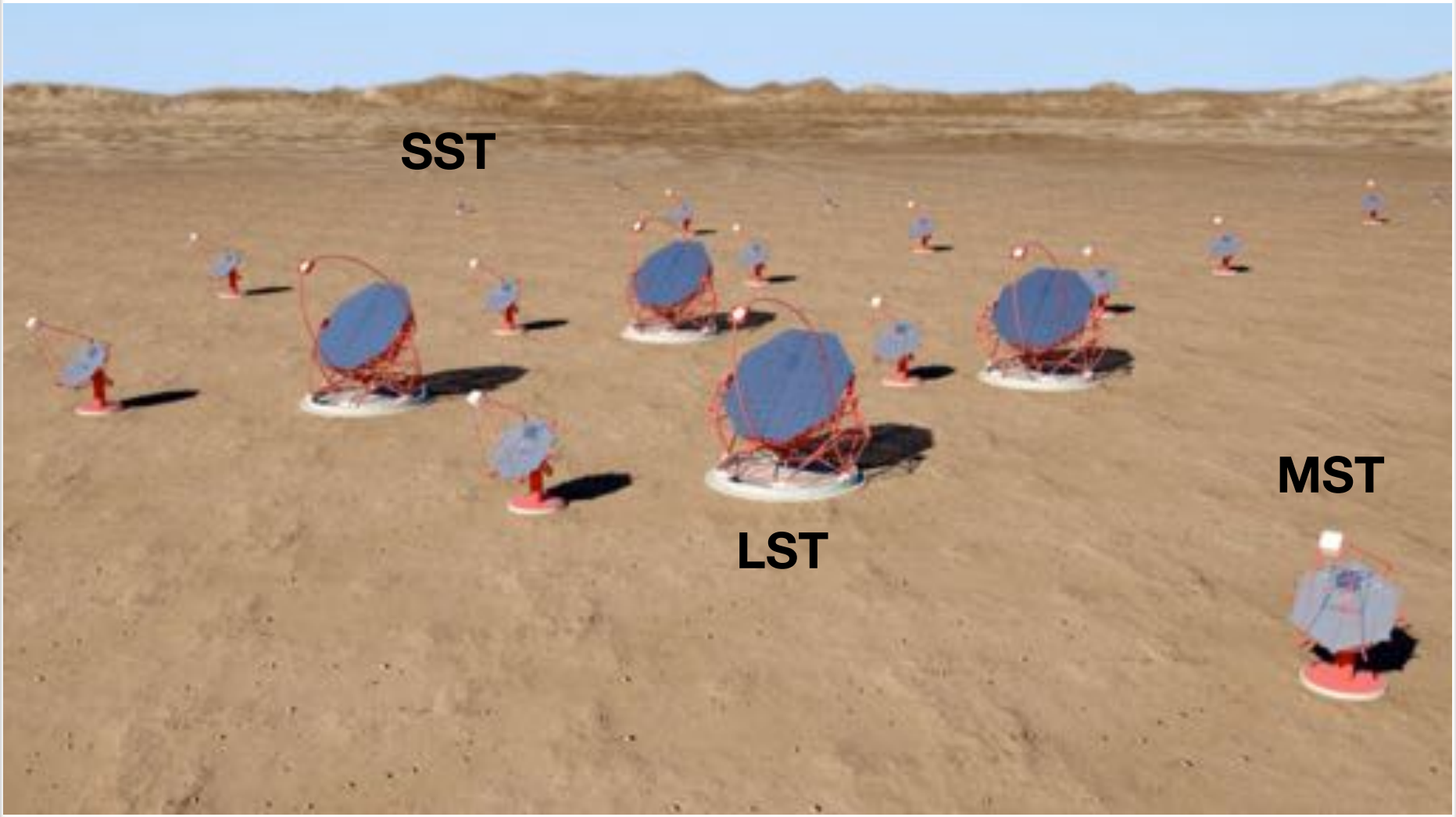

CTA SiPM Camera

- To achieve the target sensitivity, a huge R&D procedure
- Many efforts are dedicated to the development of the focal plane cameras, using novel photodetection tecnologies
- Many CTA camera will be equipped using Silicon Photomultipliers instead of PMTs

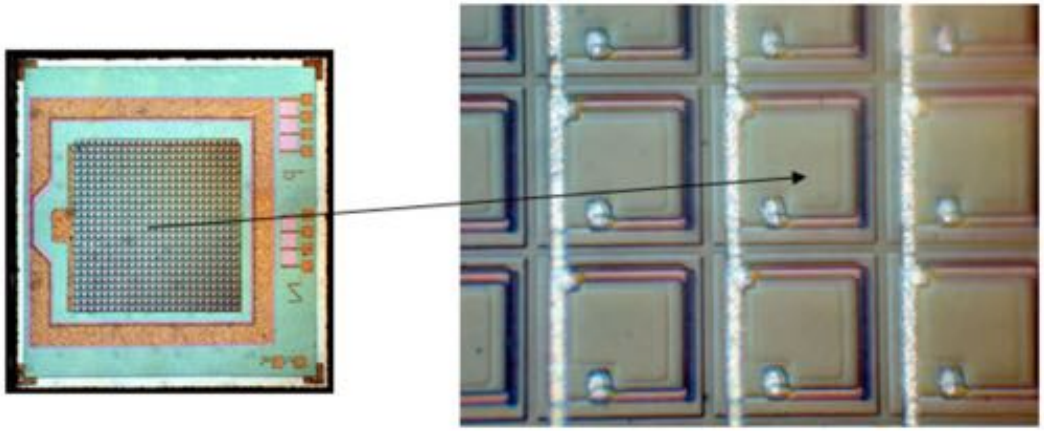

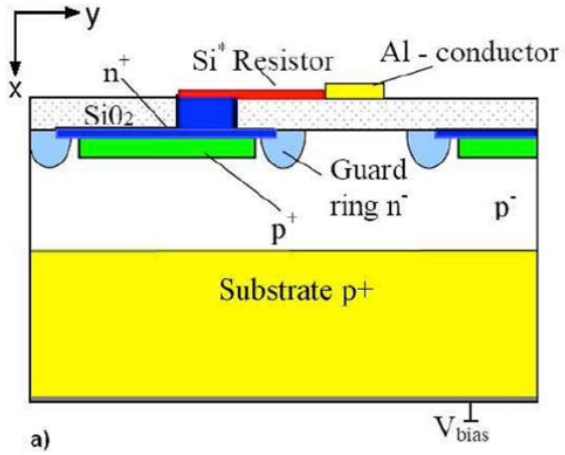

SiPM: array of microcell APD operated in geiger mode. For low intensity, the number of fired cells is proportional to the number of photons

CTA SiPM Camera

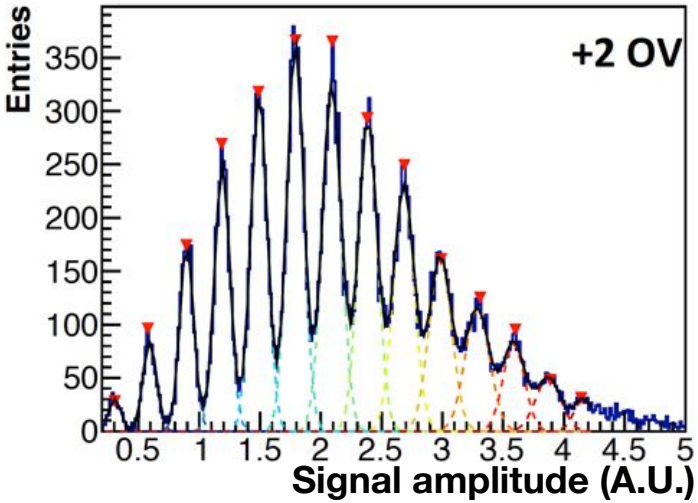

A SiPM illuminated with a laser pulse. Each peak corresponds to the number of SiPM cells that have been fired.

With respect to standard PMTs, SiPMs have a higher PDE for UV light (~50% at the peak) and can be operated also during bright moon nights without any harm on the detector → the Cherenkov light collection efficiency and the detector duty cicles are improved.

They however have a much higher intrinsic thermal noise (100 kHz/mm2 at maximum), that however is still below the noise induced by the flux of the diffuse night sky background (~ 0.1γ / cm^2 sr ns).

CTA SiPM Camera

A camera prototype for a MST CTA telescope is being developed in Perugia

pSCT telescope prototype

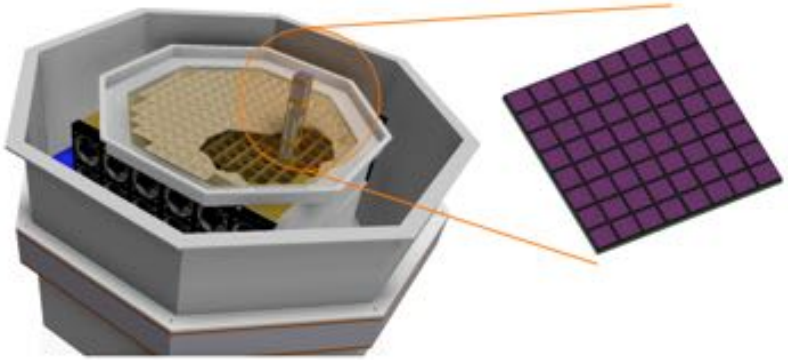

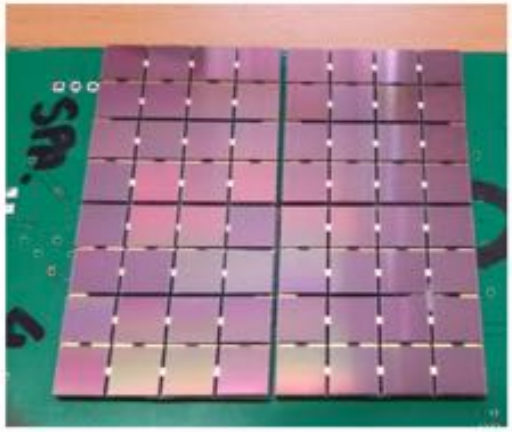

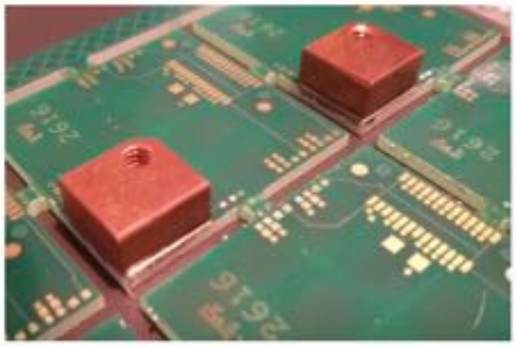

Modules composed of 16 SiPMs will be assembled and operated on the pSCT telescope (next to the VERITAS telescopes) in 2017